Supplementary Material for:

Electrochemical Ammonia Synthesis from a Bis-Aryloxy-carbene-Molybdenum Nitride Complex

Théo Personeni,[a][b]α Xueli Wang,[a]α Julien Babinot,[a] Sousanna Azar,[c] Malo Duquesnoy,[a] Stéphane Bellemin-Laponnaz,[c] Nathalie Saffon-Merceron,[d] Marie Fustier-Boutignon,[a] Eric Clot,[e] Christophe Bucher,[b]* Nicolas Mézailles[a]*

Contents

Reagents and solvents

Acetonitrile and dimethylformamide (anhydrous, ≥ 99,9 %) acetonitrile were purchased from Thermo Fisher Scientific (AcroSeal™ packaging) and used as received. THF and 1,2-dichloroethane (anhydrous, ≥ 99.9 %, inhibitor free) was purchased from Sigma-Aldrich and Thermo Fisher Scientific (AcroSeal™ and Sure/Seal™ packaging) and purified over activated alumina before use. (anhydrous, ≥ 99,9 %), HCl (2 M in Et_2O), and acetonitrile (anhydrous, ≥ 99,9 %) were purchased from Sigma-Aldrich and Thermo Fisher Scientific (AcroSeal™ and Sure/Seal™ packaging) and used as received. Tetra-n-butylammonium bis-trifluoromethanesulfonimidate (TBATFSI) was synthesized from tetrabutylammonium hydroxide (40 % weight solution in water, Sigma-Aldrich) and lithium bis-trifluoromethanesulfonimidate (99.95 %, Sigma-Aldrich), recrystallized several times in EtOH (absolute)/H_2O then dried at 50-60 °C under vacuum before use. [**H_3L**]Cl, [**$Mo^{(VI)}$**] and LutHOTf were synthesized according to previously reported literature procedures.[1,2]

Materials

Electrochemical measurements were carried out using a Biologic SP-300 potentiostat equipped with a ±1A/±48 V booster. All studies were conducted in a custom-made, single-compartment, three-electrode cell inside a nitrogen-filled glovebox. An automatic ohmic drop compensation procedure was systematically implemented when using cyclic voltammetry. Cyclic voltammetry measurements were recorded at a glassycarbon electrode (Ø = 3 mm, ALS instruments). Voltamperometry measurements at rotating disk electrodes (RDE) were carried out with a radiometer (CTV101 radiometer analytical) equipment at a rotation rate of 500 rad min^{-1} using a glassy carbon RDE tip (Ø= 3 mm). Working electrodes were systematically polished before use with diamond paste (average diameter of particles: 2 µm, PRESI SA). All measurements (analyses and electrolyses) were concucted using a reference electrode made of a silver wire dipped in a solution of silver nitrate (10^{-2} M $Ag(NO_3)$ in CH_3CN $TBAPF_6$ 0.1 M). A glass guard filled with electrolyte was used to avoid leaks of silver ions inside the electrolytic solution. The counter electrode used for all analytical studies was a Pt wire. Electrolyses were conducted in a home-made divided cell using freshly cut carbon foam (vitreous carbon foam 3000C VC003837 obtained from goodfellow) average dimensions: 1 cm x 1 cm) as a working electrode connected by a rod of glassy carbon. The counter electrode was a rod of graphite. A magnetic bar was introduced to stir the solution during electrolysis.

Spectroscopic measurements were conducted using a UV-NIR Zeiss MCS-601 spectrophotometer using a quartz immersion probe (Helmma, optical path 1 mm), or with quartz cuvettes (MB-Thuet, optical path 1 mm or 2 mm). ^{1}H and ^{13}C NMR data were collected on a Bruker Advance 300 MHz (121.5 MHz for ^{31}P, 96 MHz for ^{11}B) using valved NMR tubes purchased from Norell.

Electrochemical procedures

Typical procedures for cyclic voltammetry

Inside a N_2-regulated glove box, a freshly prepared solution of TBATFSI (0,1 M, 106 mg) in 2 mL of dry acetonitrile was introduced inside four necks, one compartment electrochemical cell containing a polished working electrode (glassy carbon, Ø: 3 mm), a platinum wire counter electrode and an Ag^+/Ag reference electrode (separated from the solution by a glass guard filled with an acetonitrile/TBATFSI solution). The purity of the electrolyte was first checked by conducting CV measurements over the accessible potential range (– 3.0 V and + 1.4 V). Then the species under study was added as a solid to reach a 1 mM concentration. The working electrode was systematically polished/washed with THF between all measurements. The reference electrode was calibrated at the end of all studies using ferrocene as an internal standard.

Typical procedures for electrocatalysis experiments

All manipulations were conducted inside a N_2-regulated glove box. Control potential electrolysis was conducted in a home-made one compartment cell containing 5 mL of a 0.1 M solution of TBATFSI or Tetrabutylammonium iodide(TBAI) (262.5 mg or 184.6 mg) in acetonitrile, 3.4 mg of [**22**^{VI}] (1 mM) and 50 equivalents of LutHOTf (64.3 mg). Cyclic voltammograms (CV) were systematically recorded before and after addition of the reactants over the accessible potential range (– 3.2 V to + 1.4 V) to check the purity of the samples. A piece of glassy carbon foam (1 x 1 cm) was used as working electrode and a large piece of graphite placed in a guard filled with a solution of ACN + TBATFSI was used as a counter electrode. A magnetic bar was introduced to stir the mixture. Electrolysis was conducted in potentiostatic regime, which involved setting the potential of the working electrode and recording the charge during the whole experiment. The electrolysis was stopped after reaching a given charge or when the measured current became negligible (stabilized charge or current < 6 % of its initial value). The advancement of the reaction was followed by conducting RDE and CV measurements on the electrolyzed solution. 0.2 mL aliquots of the crude post-electrolysis solution were transferred to a J. young tube. 0.05 mL of a 1 M HCl/Et_2O solution were added to the solution inside the J. young tube and the solvent is evaporated under vacuum. Then 0.5 mL of a 10 mM 1,3,5-trimethoxybenzene solution in DMSO-d_6 is added on the residue and a ^1H NMR spectrum (300 MHz, 64 scans) is acquired. Ammonium chloride concentration was calculated using a calibration curve.

Determination of the equilibrium constants K_1 and K_2.

The equilibrium constants K_1 and K_2 were determined by the quantification of the amount of chloride ions before and after the controlled potential electrolysis of [**1**] in the cathodic domain. The amount of chloride ions was determined by constructing a calibration curve.

- Calibration curve construction: In a 4-neck homemade electrochemical cell, with a platinum wire as a counter electrode and an Ag^+/Ag reference electrode, TBATFSI (156.8 mg, 0.1 M) is dissolved in 3 mL acetonitrile. A solution of tetrabutylammonium chloride (TBACl) (16.7 mg, 0.03 M) is prepared in acetonitrile (2 mL). Several 10 µL aliquots of this solution are then added to the TBATFSI solution (range: 0.1-1 mM). RDE measurements (500 rpm, 10 $mV.s^{-1}$) are acquired after each addings. The calibration curve is constructed by reporting the plateau current obtained by RDE measurements *vs*. the concentration of TBACl (Figure S4).

- Determination of K_1: In a 4-neck homemade electrochemical cell, with a platinum wire as a counter electrode and an Ag^+/Ag reference electrode, TBATFSI (156.8 mg, 0.1 M) is dissolved in 3 mL acetonitrile. [**1**] (2.01 mg) is then added as the solid to the TBATFSI solution to reach a 1 mM concentration. An RDE measurement (500 rpm, 10 $mV.s^{-1}$) is then recorded in the anodic domain and the plateau current of the wave at $E_{1/2}$ = + 0.7 V is determined. The concentration of chloride ions is determined using the calibration curve and K_1 is calculated using the formula $C_{Cl}^2/(1-C_{Cl})$ were C_{Cl} is the concentration of chloride determined using the calibration curve.

- Determination of K_2: using the same solution as above [**1**] (1 mM) is submitted to a control potential electrolysis (CPE) (E_{app} = − 1.0 V, see general considerations for the classic procedure for controlled potential electrolysis). After CPE, an RDE measurement (500 rpm, 10 $mV.s^{-1}$) is then recorded in the anodic domain and the plateau current of the wave at $E_{1/2}$ = + 0.7 V is determined. The concentration of chloride ions is determined using the calibration curve and K_2 is calculated using the formula $C_{Cl}^2/(1-C_{Cl})$ were C_{Cl} is the concentration of chloride determined using the calibration curve.

(Spectro)electrochemical monitoring of the disproportionation reaction

Inside a N_2 regulated glovebox a home-made one compartment electrochemical cell is filled with a 5 mL solution of TBATFSI (0.1 M; 262.5 mg) in acetonitrile containing a polished working electrode (vitreous carbon, Ø: 3 mm), a platinum wire or platinum sheet counter electrode and an Ag^+/Ag or a reference electrode (separated from the solution by a glass guard filled with a TBATFSI solution in acetonitrile). Cyclic voltammograms (CV) are then acquired to the purity of the solution over the accessible potential range. [**1**] was added as a solid to reach a 1 mM concentration. CV and rotating disk electrode (RDE) voltammograms are then acquired to assess the purity of the complex. Controlled-

potential exhaustive electrolysis is then performed using a flame-cleaned platinum grid as the working electrode and a large piece of graphite placed in a guard filled with a solution of ACN + TBATFSI was used as a counter electrode. The potential is set at –1.0 V (*vs*. $Ag^+(10^{-2}M)/Ag$). The electrolysis was stopped after reaching a given charge or when the measured current became negligible (stabilized charge or current < 6 % of its initial value). The formation of [**1**]$^-$ was assessed by CV and RDE measurements. A solution of 2,6-Lutidinium chloride (75 mg, 0.13 M) in 4 mL acetonitrile is then prepared and 40 µL of this solution is added on [**1**]$^-$. The reactivity of [**1**]$^-$ is then monitored by UV-visible absorption spectroscopy using a probe (optical path: 1 mm) inserted directly in the electrolytic solution. The acquisition is stopped when the UV-visible absorption stays constant. CV and RDE measurements are then acquired and show the presence of both [**1**] and [**4**].

Conversion of [1] in [4]

On the equimolar solution of [**1**] and [**4**] (*circa* 0.5 mM each) in acetonitrile (TBATFSI 0.1 M) 40 µL of the previously made 2,6-Lutidinium chloride solution in acetonitrile (0.13 M) is added. CV, RDE and UV-visible absorption are then acquired prior to the electrolysis. Controlled-potential exhaustive electrolysis is then performed using a piece of vitreous carbon foam (1 x 1 cm) as a working electrode and a large piece of graphite placed in a guard filled with a solution of ACN + TBATFSI was used as a counter electrode. The potential is set at –0.9 V (*vs*. $Ag^+(10^{-2}M)/Ag$). The electrolysis was stopped after reaching a given charge corresponding to 1 e^-/mole of [**1**]. Full conversion of [**4**] is then confirmed by CV, RDE and UV-visible absorption spectroscopy measurements.

Conversion of [1] in [7]$^-$

Method A) Adding 50 equivalents of LutHCl: On the previous [**4**] solution (1 mM) in acetonitrile (TBATFSI 0.1 M) is added 50 equivalents LutHCl (35.9 mg). CV, RDE and UV-visible absorption spectroscopy measurements (either using a 1 mm optical path cuvette or a probe) are then acquired and the reaction is followed by UV-visible absorption measurements. CV and RDE measurements are then acquired after 1 h.

Method B) Adding $LutHPF_6$ then TBACl. On a [**4**] solution (1 mM), formed following the protocol described above but replacing LutHCl by $LutHPF_6$, in acetonitrile (TBATFSI 0.1 M) is progressively added 50 equivalents of $LutHPF_6$. CV, RDE and UV-visible absorption spectroscopy measurements are acquired after each addition to follow the reaction. 50 equivalents of TBACl (69.5 mg) are then added to the electrolytic solution and CV, RDE and UV-visible absorption spectroscopy measurements are acquired.

Electroreduction of [**7**]$^{-}$

Controlled potential electrolysis was performed on the [**7**]$^{-}$ solution (1 mM) in acetonitrile (TBATFSI 0.1 M) formed by adding 50 equivalents of LutHCl on [**4**] using a piece of vitreous carbon foam (1 x 1 cm) as a working electrode and a large piece of graphite placed in a guard filled with a solution of ACN + TBATFSI was used as a counter electrode. The potential is set at −1.3 V (*vs*. $Ag^{+}(10^{-2}M)/Ag$). The electrolysis was stopped when the measured current became negligible (or current < 6 % of its initial value). CV, RDE and UV-visible absorption spectroscopy measurements are then acquired after the electrolysis to characterized the species formed.

Ammonium NMR calibration curve

A calibration curve was constructed by adapting a protocol published by Peters *et col*.[3] A 0.019 mol.L^{-1} stock solution of ammonium chloride was prepared by dissolving 1 mg NH_4Cl in 1 mL DMSO-d_6. Then a 10 mM 1,3,5-trimethoxybenzene (TMB) was made by dissolving 3.36 mg TMB in 2 mL DMSO-d_6. Six NMR tubes filled with six diluted solutions were then prepared using the two stock solutions:

1 – [NH_4Cl] = 3.2 mM: 84 µL stock solution of NH_4Cl + 416 µL TMB stock solution

2 – [NH_4Cl] = 2.1 mM: 55 µL stock solution of NH_4Cl + 445 µL TMB stock solution

3 – [NH_4Cl] = 1.35 mM: 35 µL stock solution of NH_4Cl + 465 µL TMB stock solution

4 – [NH_4Cl] = 0.83 mM: 22 µL stock solution of NH_4Cl + 478 µL TMB stock solution

5 – [NH_4Cl] = 0.83 mM: 19.5 µL stock solution of NH_4Cl + 480.5 µL TMB stock solution

^{1}H NMR spectra (64 scans) are then acquired for each of these solutions. These measurements are reproduced two times in order to minimize uncertainties due to integration. Calibration curve is then done by plotting the integration (*vs*. TMB) of the ammonium chloride signal (centered at 7.2 ppm) *versus* the quantity of ammonium chloride added. The calibration curve is shown on Figure S1.

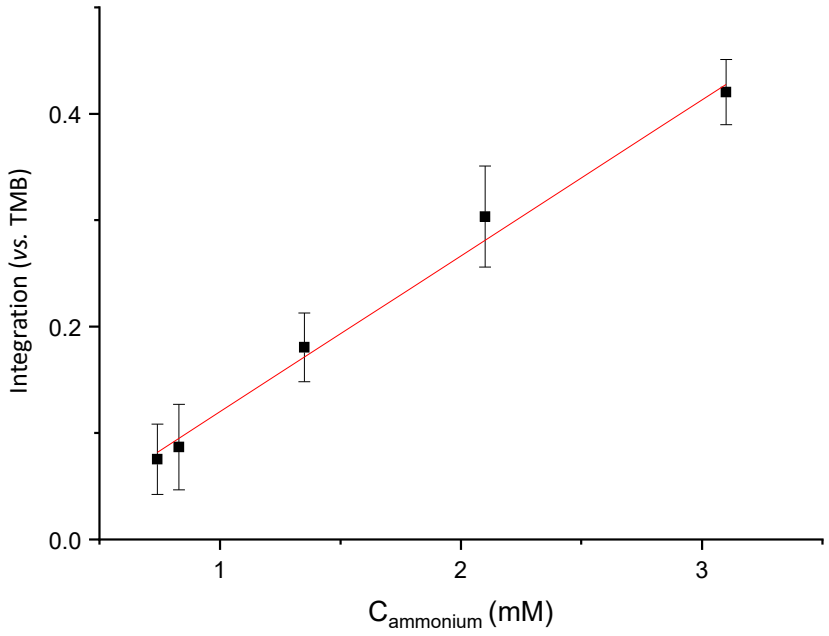

Figure S1: Ammonium concentration *vs*. ammonium signal integration (*vs*. TMB). Red: regression curve (r^2 = 0.99433).

Chemical synthesis

Synthesis of lutidinium chloride

In a round-bottom flask, lutidine (1.07 mL, 9.33 mM) was dissolved in 50 mL of *n*-pentane. The solution was cooled with an ice bath and stirred with a magnetic stirrer. Then 5.17 mL of a 2 M HCl solution in diethylether (10,3 mM) was added dropwise on the lutidine solution. A white precipitate is formed immediately after the addition of the HCl solution. The mixture is then let stir at room temperature for 10 min. The solid is then filtered, washed with 3x10 mL of *n*-pentane and dried under vacuum. Lutidinium chloride is obtained as a white powder (95.8 % yield).

^{1}H NMR (300 MHz, DMSO-d_6, 25 °C) δ: 8.35-8.29 (t, J = 9 Hz, 1 H), 7.71-7.68 (d, J = 8 Hz, 2 H), 2.72 ppm (s, 6 H) ppm.

Synthesis of lutidinium hexafluorophosphate

In a round bottom flask, lutidine (1.07 mL, 9.3 mmol) and HPF_6 (55 % w. solution in water, 1.4 mL, 9.3 mmol) is added in 5 mL of distilled water. A white precipitate forms instantaneously and the mixture is stirred for 30 minutes. The solution is then filtered and the precipitate is washed three times with THF (3x10 mL) and dried at 60 °C under vacuum for 2 days. LutHPF_6 is obtained as a white solid with 68 % yield.

^{1}H NMR (300 MHz, $CDCl_3$, 25°C) δ: 8.26-8.21 ppm (t, J = 6 Hz, 1 H); 7.61-7.55 ppm (d, J = 9 Hz, 1 H); 2.9 ppm (s, 6H).

Synthesis of [1^{VI}]

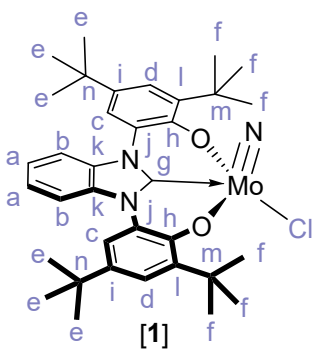

[**1**]

In a glovebox under N_2, a solution of $MoN(O^tBu)_3$ (550 mg, 1.67 mmol, 1.1 eq) in 15 mL of CH_2Cl_2 and a solution of ligand 1 (855 mg, 1.52 mmol) in 15 mL of CH_2Cl_2 were mixed in a Schlenk and stirred for 2 days at RT. The solvent was removed under vacuum till approx. 2 mL and 25 mL of pentane were added, inducing an intense precipitation. The solution was stirred for 10 min and filtered with a cannula. The solid was briefly dried under vacuum, solubilized in 2 mL of CH_2Cl_2 and precipitated again by adding 25 mL of pentane. After filtration, the product was dried overnight under vacuum, yielding a violet powder (762 mg, 75%). Monocrystals were grown from a concentrated solution of the complex

in CH_2Cl_2 layered with pentane. Anal. Calcd. for $C_{35}H_{44}ClMoN_3O_2$: C, 62.73; H, 6.62; N, 6.27. Found: C, 62.47; H, 6.37; N, 6.16.

^{95}Mo NMR (26 MHz, CD_2Cl_2): δ 256.6 ppm.

^{1}H NMR (400 MHz, CD_2Cl_2): δ 8.18 (dd, *J* = 6.3, 3.2 Hz, 2H, Ha), 7.86 (d, *J* = 2.2 Hz, 2H, Hc), 7.64 (dd, *J* = 6.4, 3.2 Hz, 2H, Ha), 7.54 (d, *J* = 2.3 Hz, 2H, Hd), 1.55 (s, 18H, Hf), 1.44 (s, 18H, He) ppm.

^{13}C NMR (100 MHz, CD_2Cl_2): δ 191.13 (Cg), 153.82 (Ch), 144.29 (Ci), 139.89 (Cj), 134.44 (Ck), 126.42 (Cb), 124.01 (Cd), 123.94 (Cl), 116.64 (Cc), 114.89 (Ca), 36.28 (Cm), 35.36 (Cn), 31.89 (Ce), 30.30 (Cf) ppm.

Synthesis of $[\mathbf{1}^{V}]^{-}$ Cp_2Co^{+}

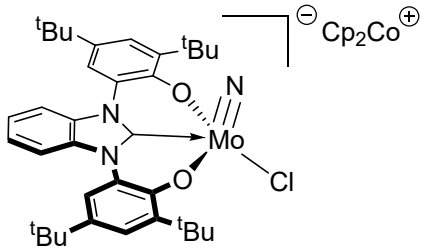

[**1**]$^{-}$

Inside a N_2 regulated glovebox, [**1**] (25 mg, 0.038 mmol) is dissolved in 1.5 mL THF. The solution is added on cobaltocene (7.05 mg, 0.038 mmol). The mixture turned instantaneously grey-brown. The solvent is then evaporated and a grey solid is obtained. The solid is then dissolved in acetonitrile-d_3 and the ^{1}H NMR spectrum is in line with the paramagnetic nature of [**1**]$^{-}$. Monocrystals suitable for XRD were grown from this saturated solution (77 % yield). Anal. Calcd. for $C_{35}H_{44}ClMoN_3O_2$, $C_{10}H_{10}Co$: C, 62.90; H, 6.33; N, 4.89. Found: C, 63.02; H, 6.25; N, 4.52.

Synthesis of complex $[\mathbf{7}^{IV}]^{-}$

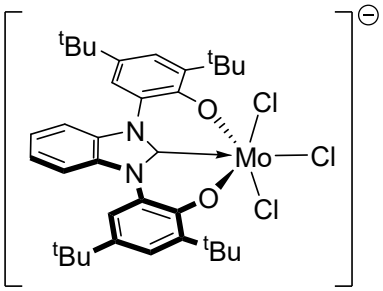

[**7**]$^{-}$

Inside a N_2-regulated glovebox, [**1**] (25 mg, 0.037 mmol) is dissolved in 5 mL acetonitrile. Then, the mixture is added on $Cr(C_6H_6)_2$ (15.5 mg, 0.075 mmol) and on LutHCl (21.4 mg, 0.15 mmol). The reaction mixture is then stirred overnight. The solution is filtered and the solvent is then evaporated under vacuum and the solid obtained is washed with 3x2 mL of dry *n*-pentane. The solid is then dried under vacuum and dissolved in $CDCl_3$. The NMR spectrum obtained is in line with the paramagnetic nature of the compound. Monocrystals suitable for XRD were obtained from this solution after a few days at room temperature. The supernatant is then

removed and the crystals obtained are washed with dry *n*-pentane. [**7**]$^{-}$ is obtained as a red crystalline solid (69 % yield). Crystals were used to perform cyclic voltammetry experiments and EPR and UV-visible spectroscopy measurements. Anal. Calcd. for $C_{35}H_{44}Cl_3MoN_2O_2$, $C_{12}H_{12}Cr$, 2($CDCl_3$), 2(CH3CN): C, 50.60; H, 5.29; N, 4.45. Found: C, 50.20; H, 5.66; N, 5.10.

Synthesis of complex [7^{V}]

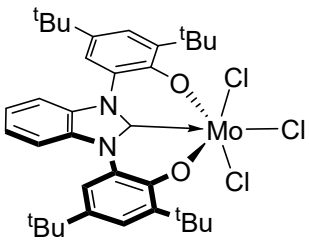

[7^{V}]

Inside a N_2-regulated glovebox, [**1**] (536 mg, 0.8 mmol) is dissolved in 5 mL THF. Then, PCl_5 (333 mg, 1.6 mmol) is added to the mixture. The purple solution was then allowed to stir for 2.5 h. After removal of the solvent under vacuum, the residual solid was washed with pentane (3 mL) for 3 times. Monocrystals suitable for XRD were obtained from the mixture of THF/Pentane after a few days at -35 °C. [**7**^{V}]$^{-}$ is obtained as a brown crystalline solid (71 % yield). Anal. Calcd. for $C_{35}H_{44}Cl_3MoN_2O_2$, C_4H_8O: C, 58.61; H, 6.56; N, 3.51. Found: C, 58.47; H, 6.61; N, 3.50.

Synthesis of complex [$8^{V\text{-}IV}$]$^{-}$

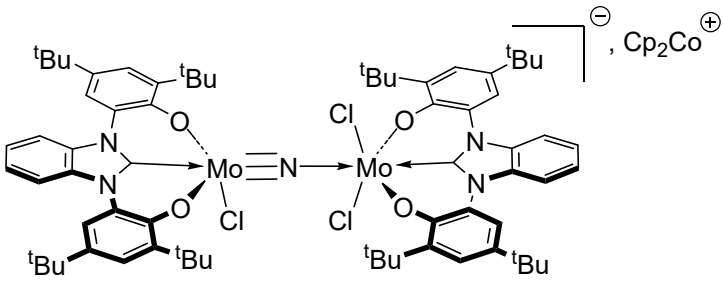

[**8**]$^{-}$

Inside a N_2-regulated glovebox, [**1**] (25 mg, 0.037 mmol) is dissolved in 3 mL THF. The solution is then added on cobaltocene (15.2 mg, 0.075 mmol) and LutHCl (16.1 mg, 0.12 mmol). The mixture is stirred overnight. The reaction mixture is then filtered and the solvent is evaporated under vacuum. The solid obtained is washed with 3x2 mL of dry *n*-pentane, and the solid is then dried under vacuum. The solid is dissolved in 1 mL THF. Monocrystals suitable for XRD were grown by vapor diffusion of heptane in the THF solution.

Electrochemical data

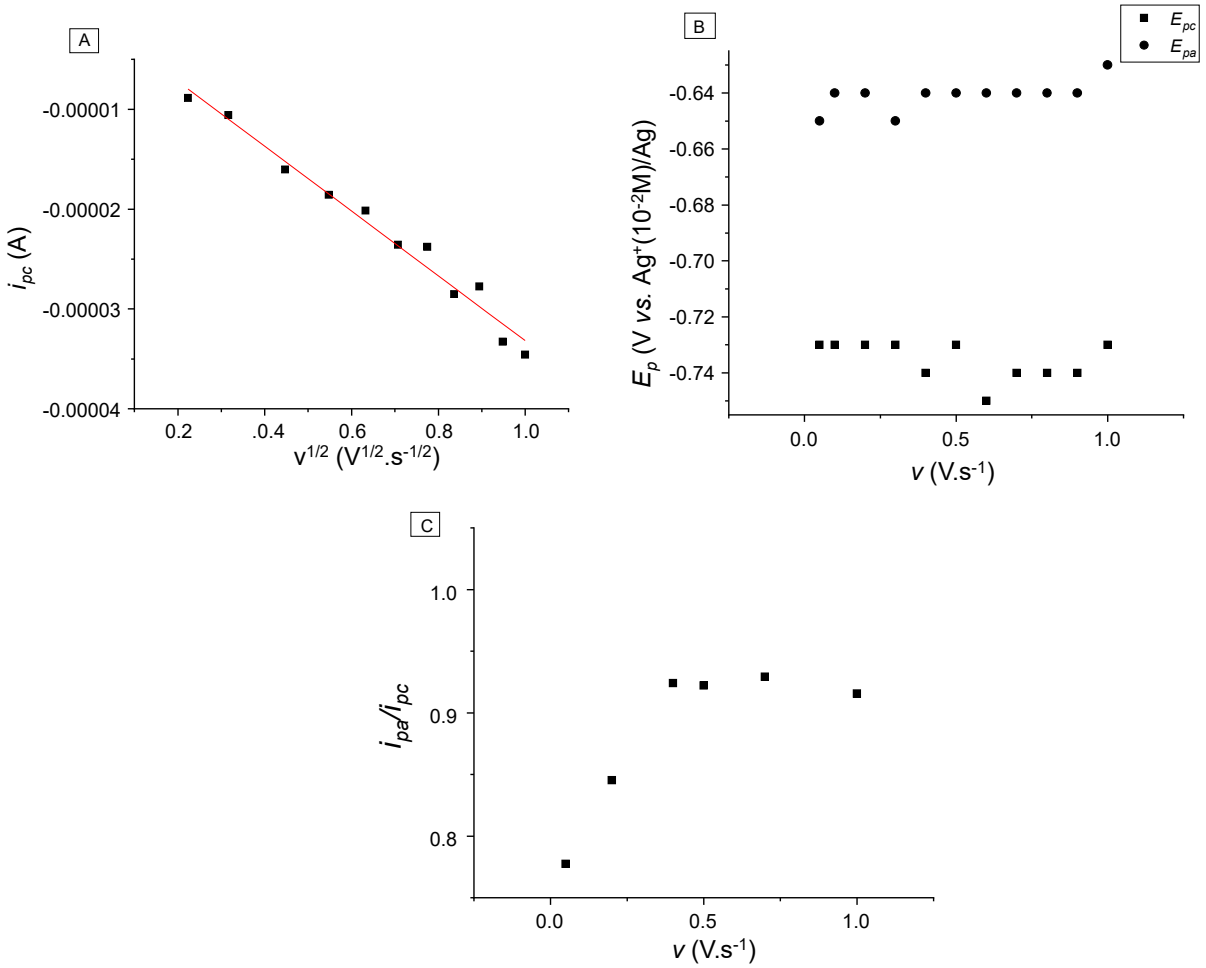

Figure S2: A) variation of the cathodic peak intensity of [**1**] (1 mM) in acetonitrile with the square root of the scan rate (red: fitting curve) B) Variation of the cathodic (squares) and anodic peak potential (circles) of [**1**] (1 mM) in acetonitrile with the scan rate. C) variation of the ratio of the anodic and the cathodic peak current of [**1**] (1 mM) in acetonitrile with the scan rate (red: fitting curve). Acetonitrile + TBATFSI 0.1 M. Working electrode: GC (Ø: 3 mm), reference electrode: $Ag^+(10^{-2}$ M)/Ag, counter electrode: Pt wire

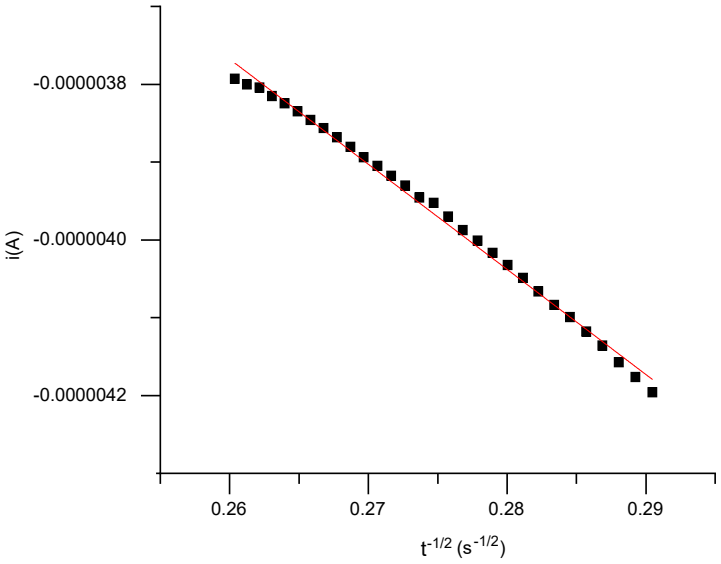

Figure S3: A) intensity *vs.* time plot of [**1**^{VI}] (1 mM) in acetonitrile (E_{app} = -1.0 V). B) Cottrell plot (i *vs.* $t^{-1/2}$) of [**1**^{VI}] (1 mM) in acetonitrile (red curve: linear fit). Acetonitrile + TBATFSI 0.1 M. Working electrode: GC (Ø: 3 mm), reference electrode: Ag^{+}(10^{-2} M)/Ag, counter electrode: Pt wire

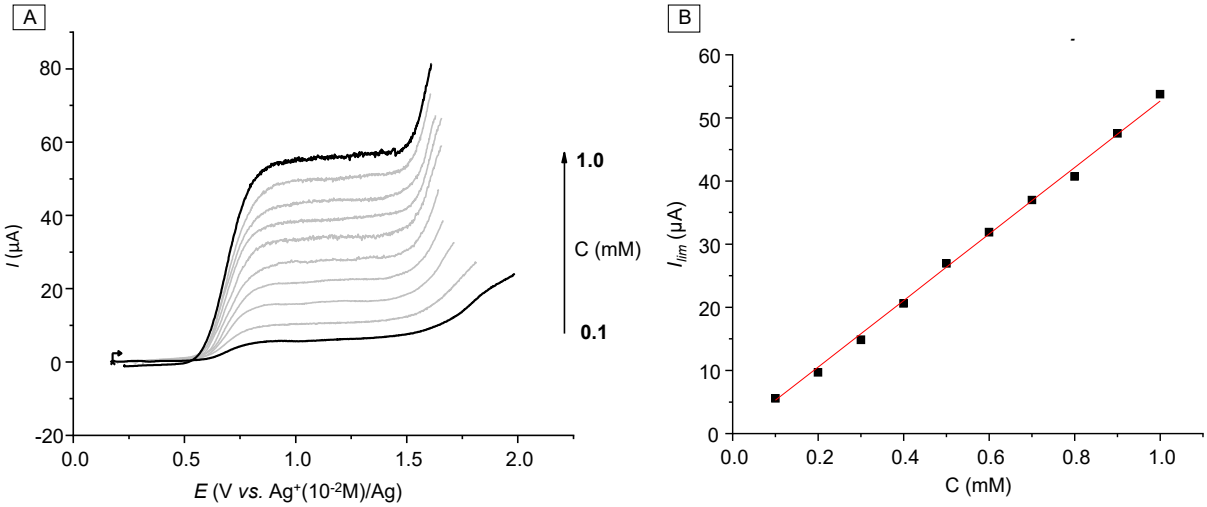

Figure S4: A) RDE voltammogram acquired for several concentration of TBACl (0.1 mM-1 mM) in acetonitrile (TBATFSI 0.1 M). B) variation of the diffusion current of the wave associated with the oxidation of chloride *vs*. the concentration of TBACl. Electrode GC (Ø: 3 mm), C = 1 mM, reference: Ag^{+} (10^{-2} M)/Ag, v: 20 mV/s RDE, 500 rpm, counter electrode: Pt.

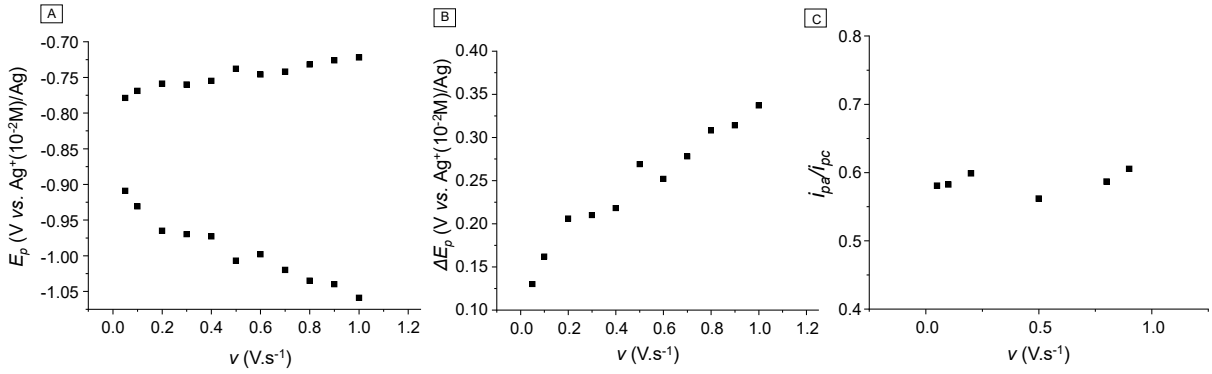

Figure S5: A) Variation of the cathodic (squares) and anodic peak potential (circles) of [**1**] (1 mM) in dimethylformamide with the scan rate. B) Variation of the peak potential difference (E_{pa}–E_{pc}) of [**1**] (1 mM) in dimethymformamide with the scan rate. C) Variation of the ratio of the anodic and the cathodic peak current of [**1**] (1 mM) in dimethylformamide with the scan rate. Dimethylformamide + TBATFSI 0.1 M. Working electrode: GC (Ø: 3 mm), reference electrode: Ag$^+$(10^{-2} M)/Ag, counter electrode: Pt wire.

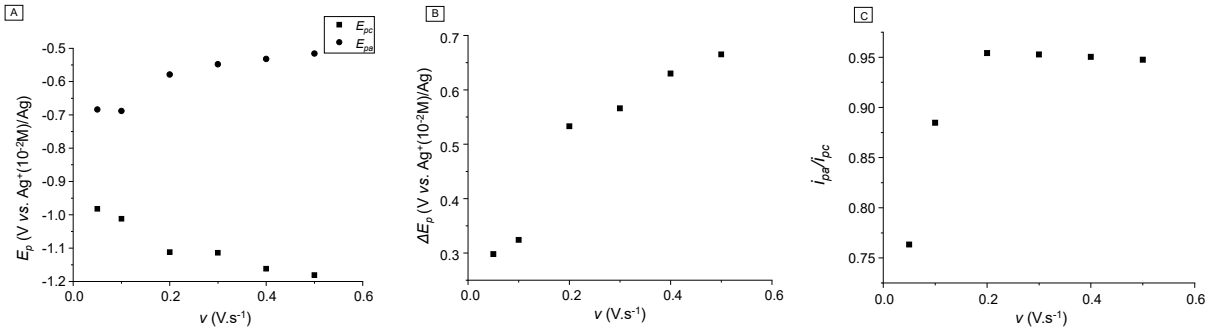

Figure S6: A) Variation of the cathodic (squares) and anodic peak potential (circles) of [**1**] (1 mM) in tetrahydrofuran with the scan rate. B) Variation of the peak potential difference (E_{pa}–E_{pc}) of [**1**] (1 mM) in tetrahydrofuran with the scan rate. C) Variation of the ratio of the anodic and the cathodic peak current of [**1**] (1 mM) in tetrahydrofuran with the scan rate. Tetrahydrofuran + TBATFSI 0.1 M. Working electrode: GC (Ø: 3 mm), reference electrode: Ag$^+$(10^{-2} M)/Ag, counter electrode: Pt wire.

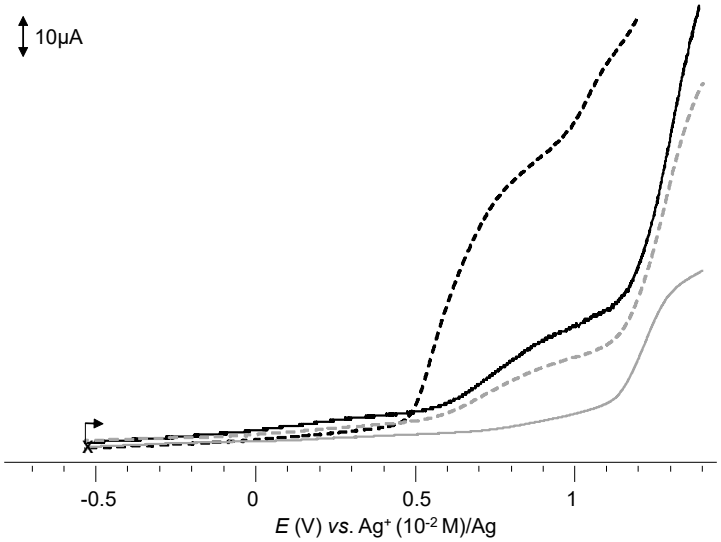

Figure S7: RDE voltammograms acquired for a solution of [**1**] (1 mM) in acetonitrile (black), 1,2-dichloroethane (grey), tetrahydrofuran (dotted grey) and dimethylformamide (dotted black) *(+*TBATFSI 0.1 M*).* Electrode GC (Ø: 3 mm), C = 1 mM, reference: Ag$^+$ (10^{-2} M)/Ag, v: 20 mV/s RDE, 500 rpm, counter electrode: Pt.

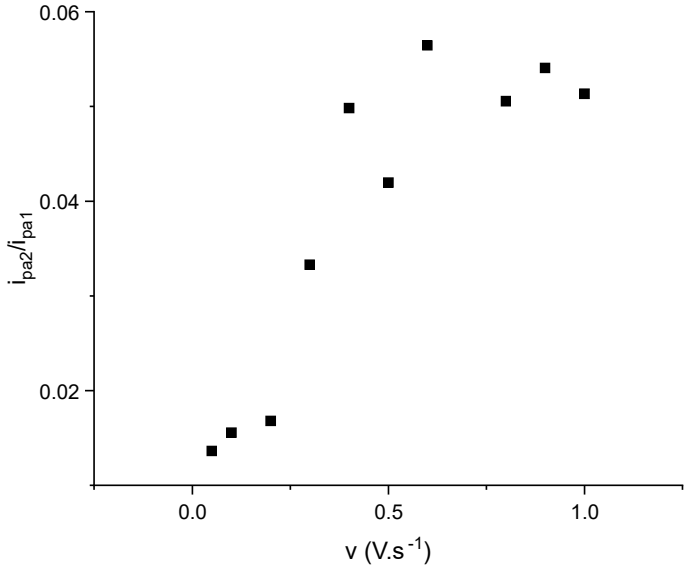

Figure S8: Variation of the peak current intensity of the oxidation wave at E_p = -0.55 V on the peak current intensity of the oxidation wave of [**1**^{V}]$^{-}$ (1 mM) *versus* the scan rate. Acetonitrile + TBATFSI 0.1 M. Working electrode: GC (Ø: 3 mm), reference electrode: Ag^{+}(10^{-2} M)/Ag, counter electrode: Pt wire.

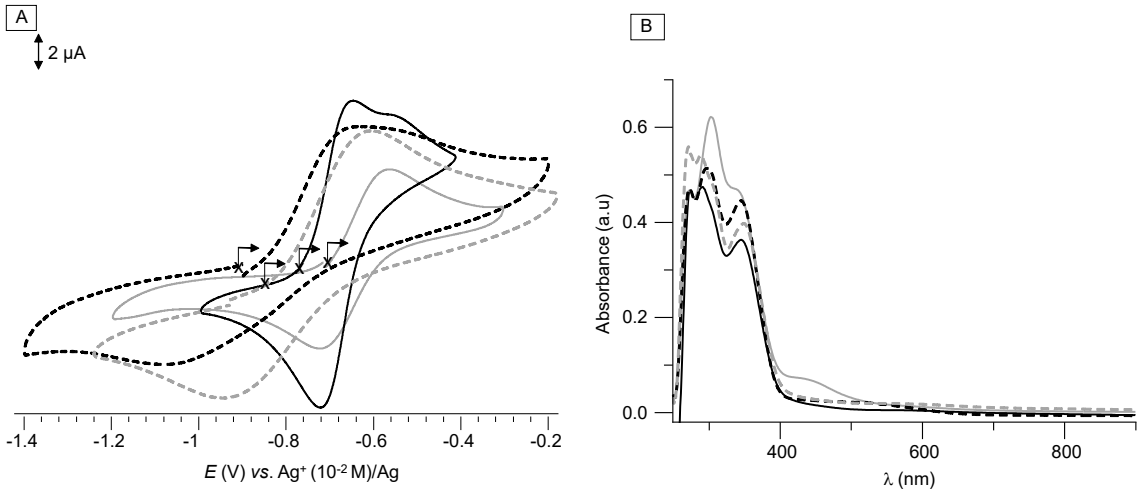

Figure S9: A) Cyclic voltammetry of [**1**] (1 mM) after exhaustive electrolysis (1e/mole) in acetonitrile (black), 1,2-dichloroethane (grey), tetrahydrofuran (dotted grey) and dimethylformamide (dotted black). B) UV-visible spectra of [**1**] (1 mM) after exhaustive electrolysis (1e/mole) in acetonitrile (black), 1,2-dichloroethane (grey), tetrahydrofuran (dotted grey) and dimethylformamide (dotted black). Acetonitrile, 1,2-dichloroethane, tetrahydrofuran, dimethylformamide + TBATFSI 0.1 M. Working electrode: GC (Ø: 3 mm), reference electrode: Ag^{+}(10^{-2} M)/Ag, counter electrode: Pt wire /carbon in acetonitrile + TBATFSI, electrolysis performed on glassy carbon foam, optical path: 1 mm.

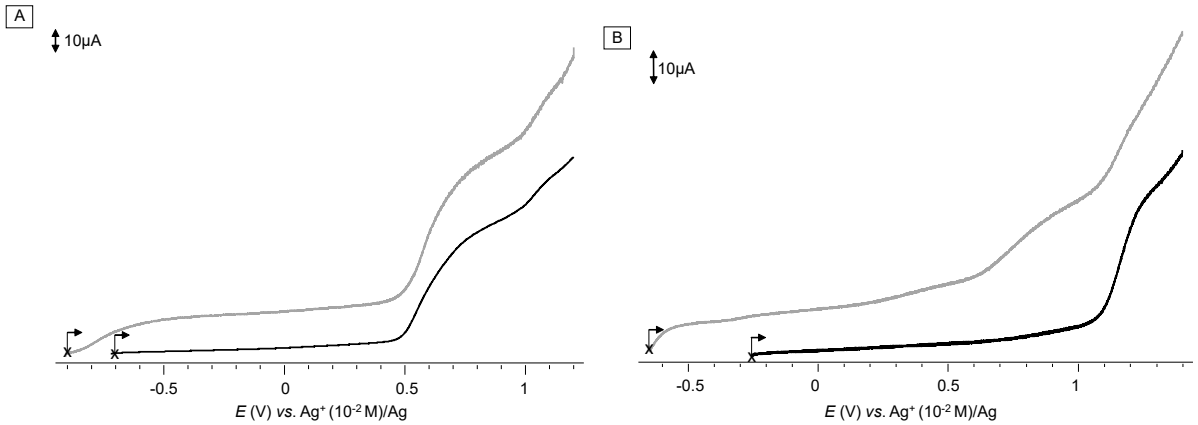

Figure S10: RDE voltammogram acquired for a solution of [**1**] (1 mM) before (black) and after (grey) controlled potential electrolysis in dimethylformamide (A) and in THF (B) (TBATFSI 0.1 M). E_{app} = –1.2 V, 1e$^-$/mole, electrolysis performed RVC foam. Electrode GC (Ø: 3 mm), C = 1 mM, reference: Ag^+ (10^{-2} M)/Ag, v: 20 mV/s RDE, 500 rpm, counter electrode: Pt.

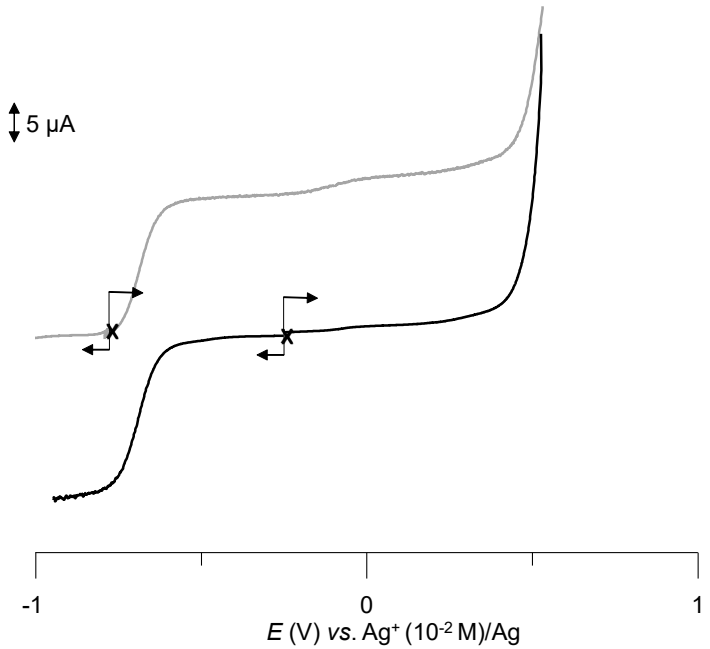

Figure S11: RDE voltammogram acquired for a solution of [**1**] (1 mM) before (black) and after (grey) controlled potential electrolysis in acetonitrile using TBACl (0.1 M) as an electrolyte. E_{app} = –1.0 V, 1e$^-$/mole, electrolysis performed RVC foam. Electrode GC (Ø: 3 mm), C = 1 mM, reference: Ag^+ (10^{-2} M)/Ag, v: 20 mV/s RDE, 500 rpm, counter electrode: Pt.

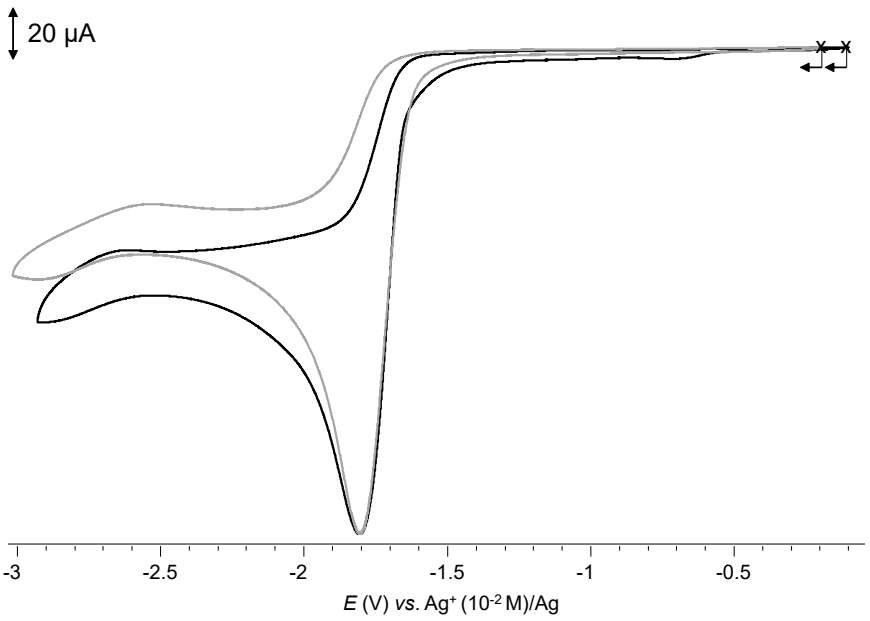

Figure S12: Cyclic voltammograms recorded for a solution of [**1**] (1mM) in presence of 50 equivalents (50 mM) of LutHOTf (black curve) in acetonitrile (TBATFSI 0.1 M) or for a solution of LutHOTf (50 mM) (grey curve) in acetonitrile (TBATFSI 0.1 M). Electrode GC (Ø: 3 mm), C = 1 mM, reference: Ag^+ (10^{-2} M)/Ag, v: 100 $mV.s^{-1}$, counter electrode: Pt.

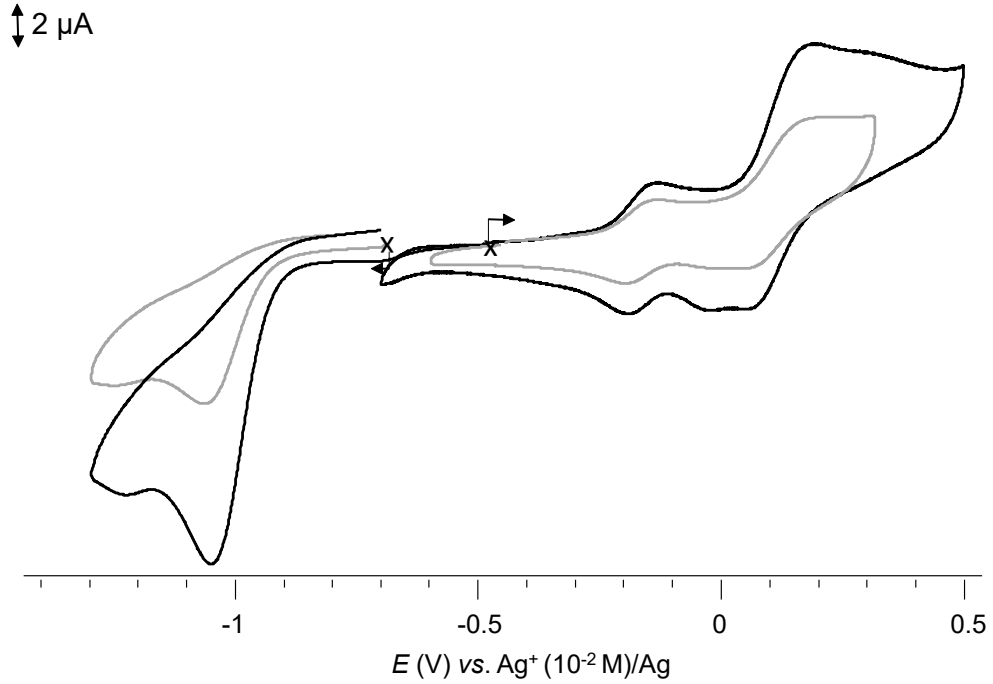

Figure S13: Cyclic voltammogram obtained for a solution of [**4**] (1 mM, formed *in situ* according to the protocol described above) in acetonitrile (TBATFSI 0.1 M) 1 h after the addition of 50 equivalents of LutHCl (black curve) or after the consecutive addition of 50 equivalents of $LutHPF_6$ then 50 equivalents of TBACl (grey curve). Electrode GC (Ø: 3 mm), C = 1 mM, reference: Ag^+ (10^{-2} M)/Ag, v: 100 $mV.s^{-1}$, counter electrode: Pt.

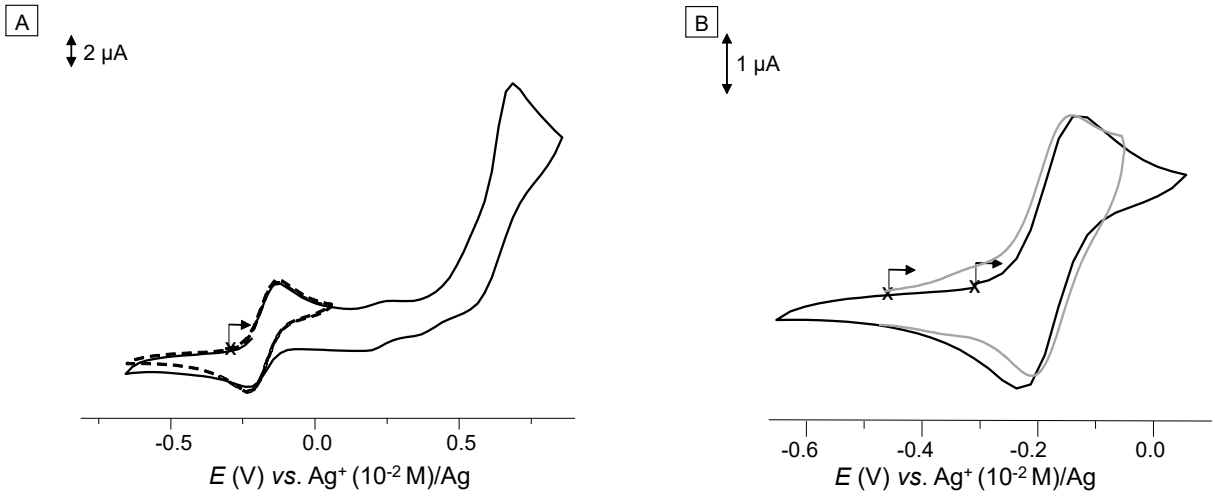

Figure S14: A) cyclic voltammogram recorded in the anodic domain for a solution of [**7**]$^-$ (1 mM) in acetonitrile (TBATFSI 0.1 M). B) cyclic voltammogram recorded for a solution of [**7**]$^-$ (1 mM, black curve) or for a solution of [**4**] (1 mM, formed *in situ* according to the protocol described above) 1 h after the addition of 50 equivalents of LutHCl (grey curve) in acetonitrile (TBATFSI 0.1 M). Electrode GC (Ø: 3 mm), C = 1 mM, reference: Ag^+ (10^{-2} M)/Ag, v: 100 mV.s^{-1}, counter electrode: Pt.

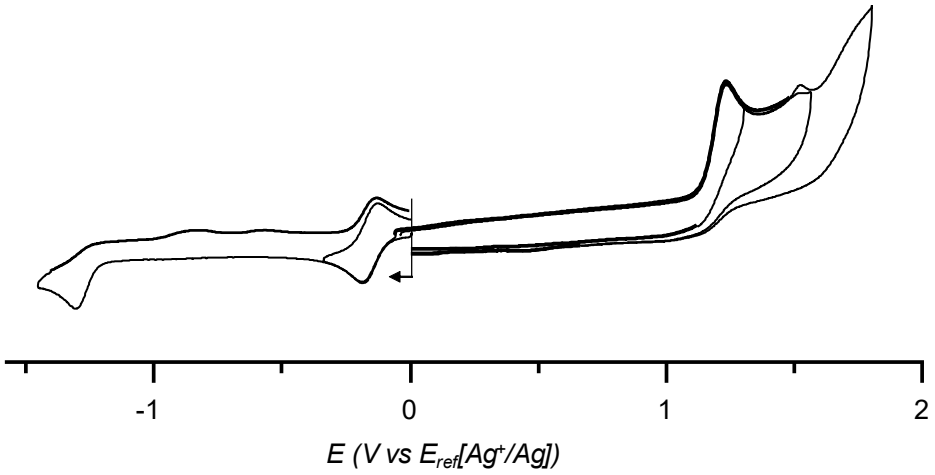

Figure S15: Cyclic voltammograms of a solution of [**7**] in ACN (TBATFSI 0.1 M). Working electrode: GC (Ø: 3 mm), reference electrode: Ag^+ (10^{-2} M)/Ag, counter electrode: Pt wire. v: 100 mV.s^{-1}

UV-visible absorption spectroscopy data

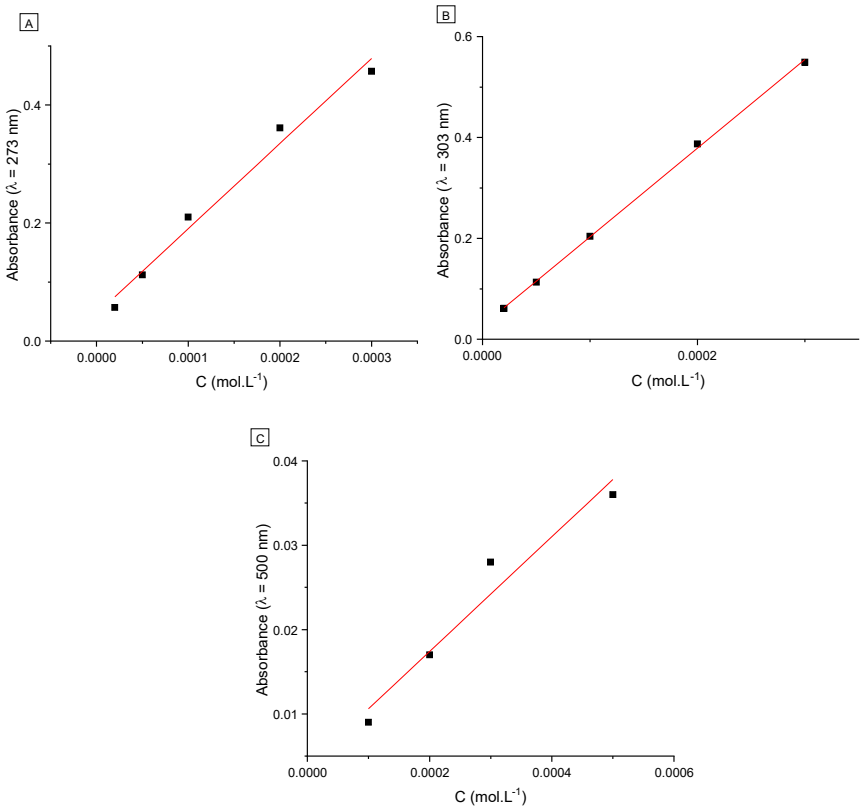

Figure S16: Beer-Lambert plots of absorbance at 273 nm (A, r^2 = 0.98292), 303 nm (B, r^2 = 0.9936) and 500 nm (C, r^2 = 0.9520) *versus* the concentration of [**1**]. Red: linear regression. Solvent: acetonitrile, optical path: 1 mm.

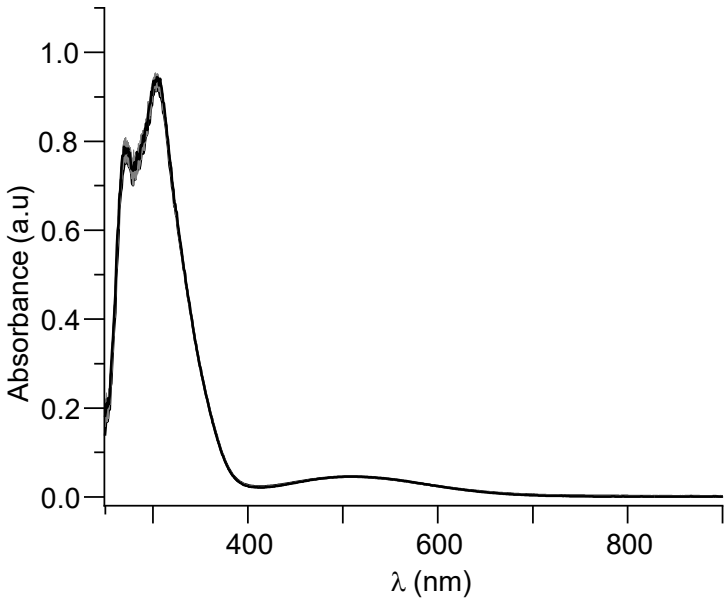

Figure S17: UV-visible absorption spectra recorded after the addition of 50 equivalents of LutHCl (50 mM) on a 1 mM solution of [**1**] in acetonitrile. Optical path: 1 mm.

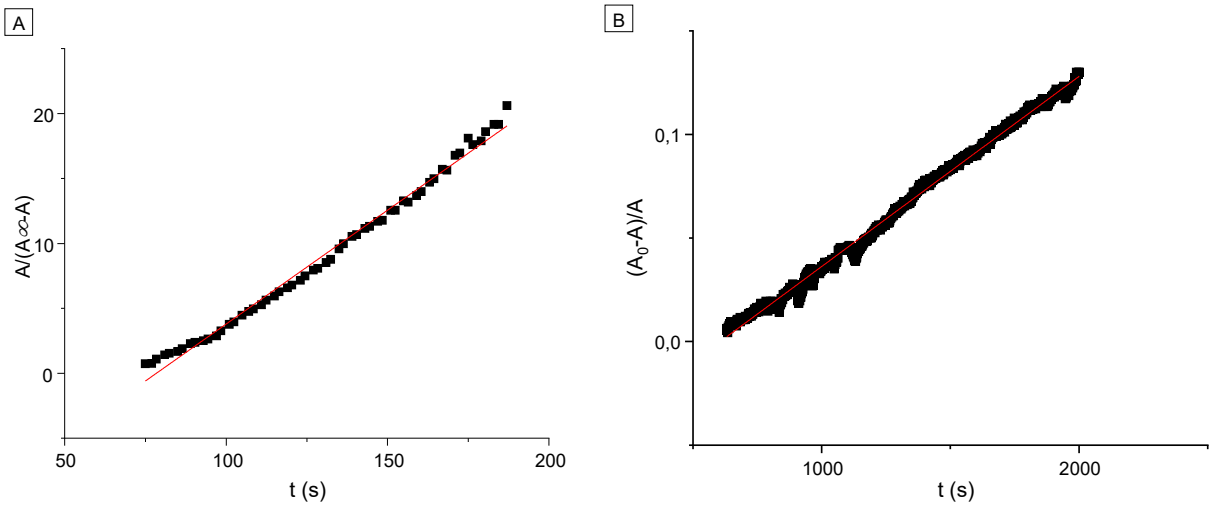

Figure S18: Following of the disproportionation process over time: 2 [**2**^{V}] → [**1**^{VI}] and [**3**^{IV}]. (A: absorbance at 450 nm, A_{∞}: final absorbance at 450 nm): A) variation of the ratio $A/(A_{\infty}-A)$. Red: linear fit, $r^2 = 0.99034$. B) variation of the ratio $A/(A_{\infty}-A)$. Red: linear fit, $r^2 = 0.99524$.

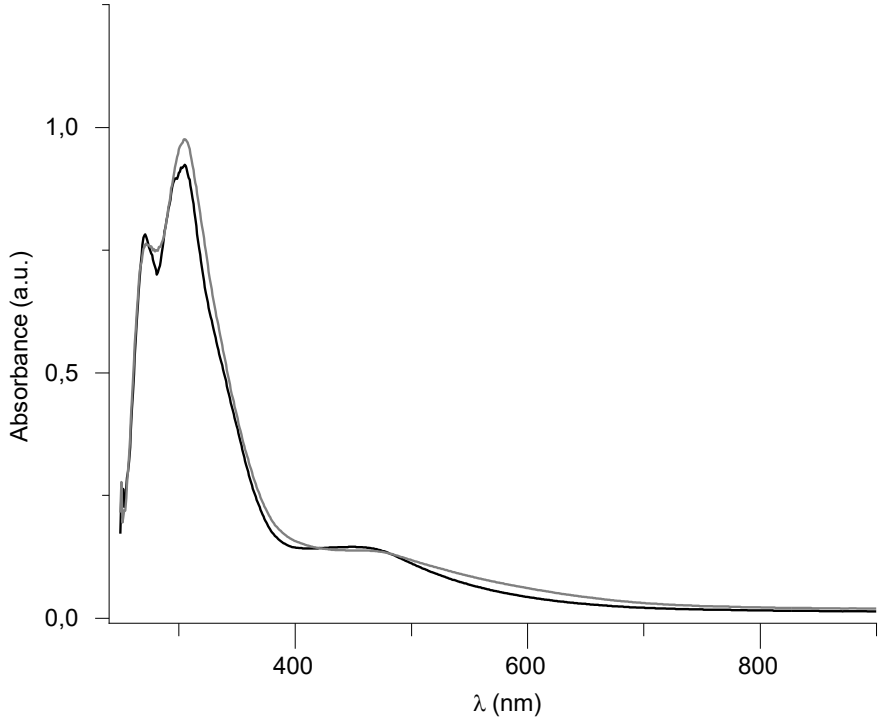

Figure S19: UV-visible absorption spectra of the equimolar mixture of [**1**] + [**3**] (0.5 mM each, formed *in situ* according to the protocol described above in acetonitrile (TBATFSI 0.1 M) before (black) and after (grey) addition of 1 mM LutHCl. Optical path: 1 mm.

EPR spectroscopy data

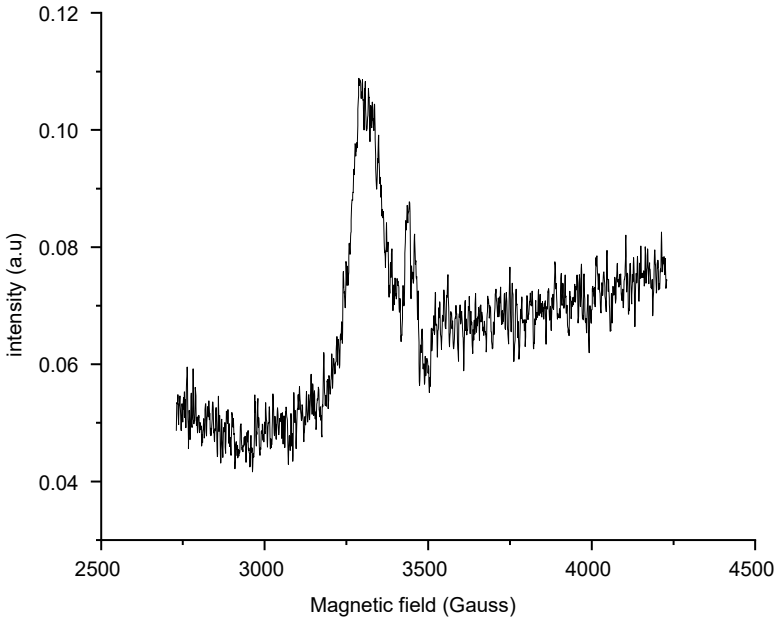

Figure S20: ESR spectrum of [**1**^{VI}] (1 mM) in acetonitrile TBAFSI 0.1 M (105 K).

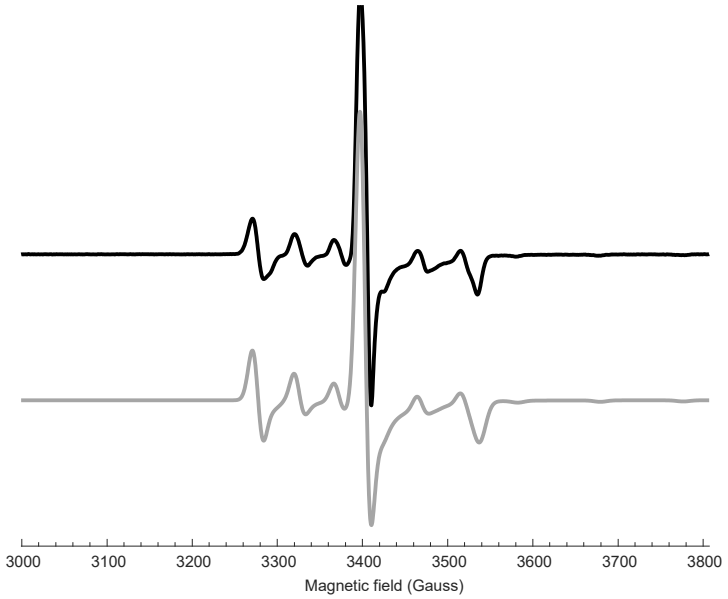

Figure S21: Experimental (black) and simulated (grey) ESR spectrum at 110 K of [**1**^{V}]$^{-}$ (1 mM) formed by exhaustive electrolysis of [**1**^{VI}] (1e/mole) in acetonitrile. Acetonitrile + TBATFSI 0.1 M. Working electrode: GC (Ø: 3 mm), reference electrode: $Ag^{+}(10^{-2}$ M)/Ag, counter electrode: Pt wire/carbon in acetonitrile + TBATFSI, electrolysis performed on glassy carbon foam.

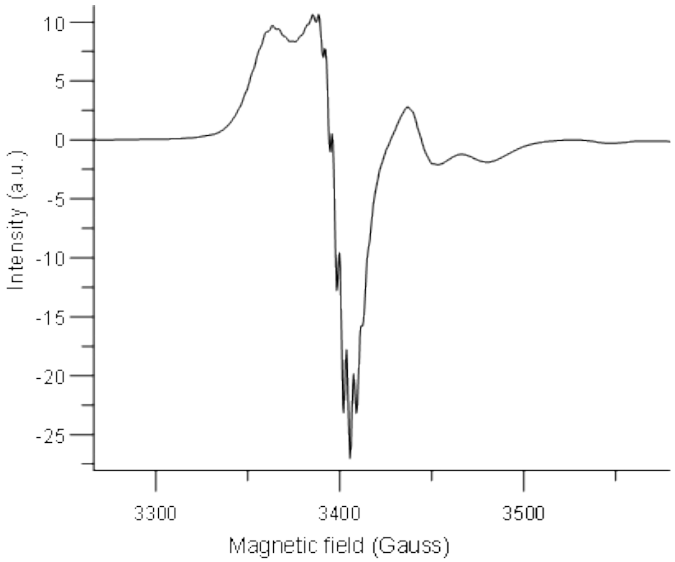

Figure S22: X-band EPR spectrum recorded for a frozen solution of complex $[\mathbf{7}^{IV}]^{-}$ $Cr(C_6H_6)_2^{+}$ (120 K, 1 mM in acetonitrile). The intense signal centered at g = 1.99 exhibiting hyperfine coupling constants is characteristic of bis(benzene)chromium cation.[5]

Parameter	**Value**
g_x	1.985
g_y	1.983
g_z	1.907
A_x (G)	47
A_y (G)	47
A_z (G)	90.5

Table S1*:* Calculated parameter for the spectrum (X-band) at 120 K of $[\mathbf{1}^{V}]^{-}$ at 1 mM in THF TBATFSI 0.1 M after exhaustive electrolysis, using Easy Spin (Matlab toolbox).[34] Electrolysis: woking electrode: Pt, E_{app} = -1 V, 5 mL.

NMR data

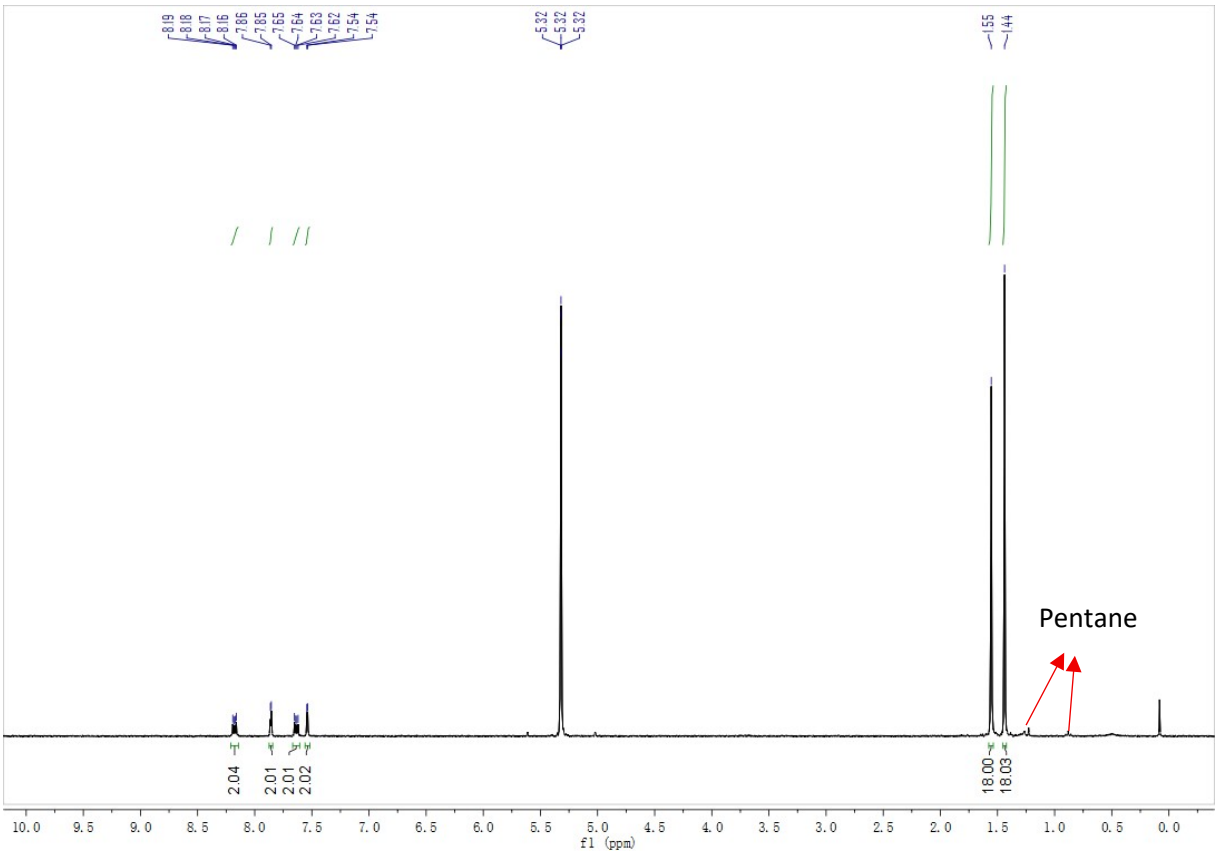

Figure S23: ^{1}H NMR (400 MHz) spectrum of [**1**] in CD_2Cl_2.

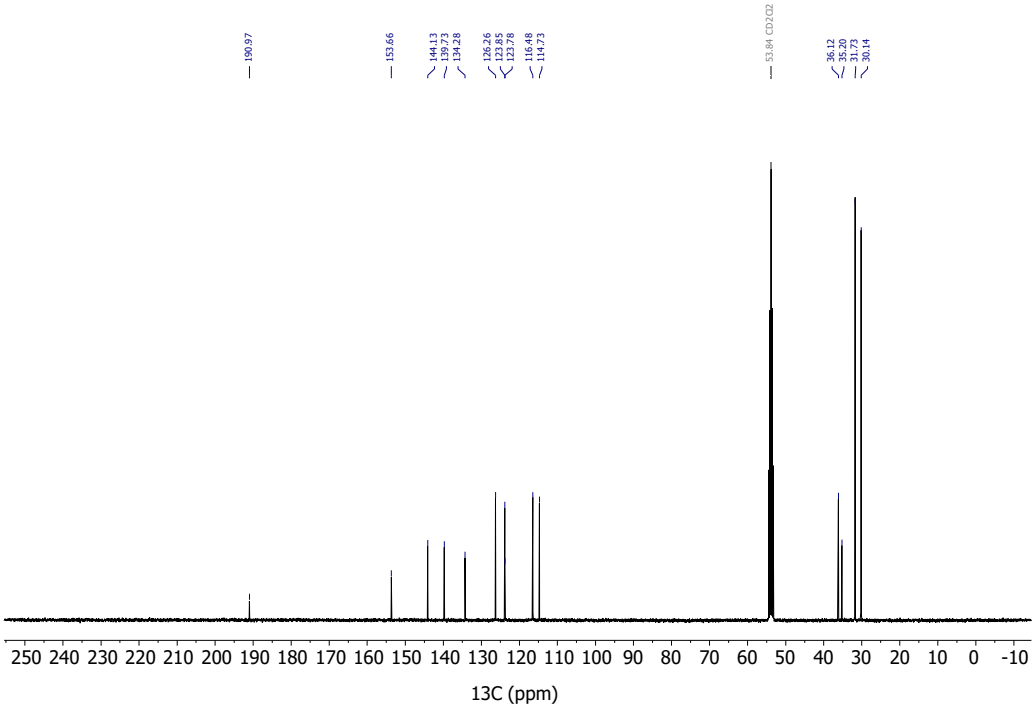

Figure S24: ^{13}C NMR (100 MHz) spectrum of [**1**] in CD_2Cl_2.

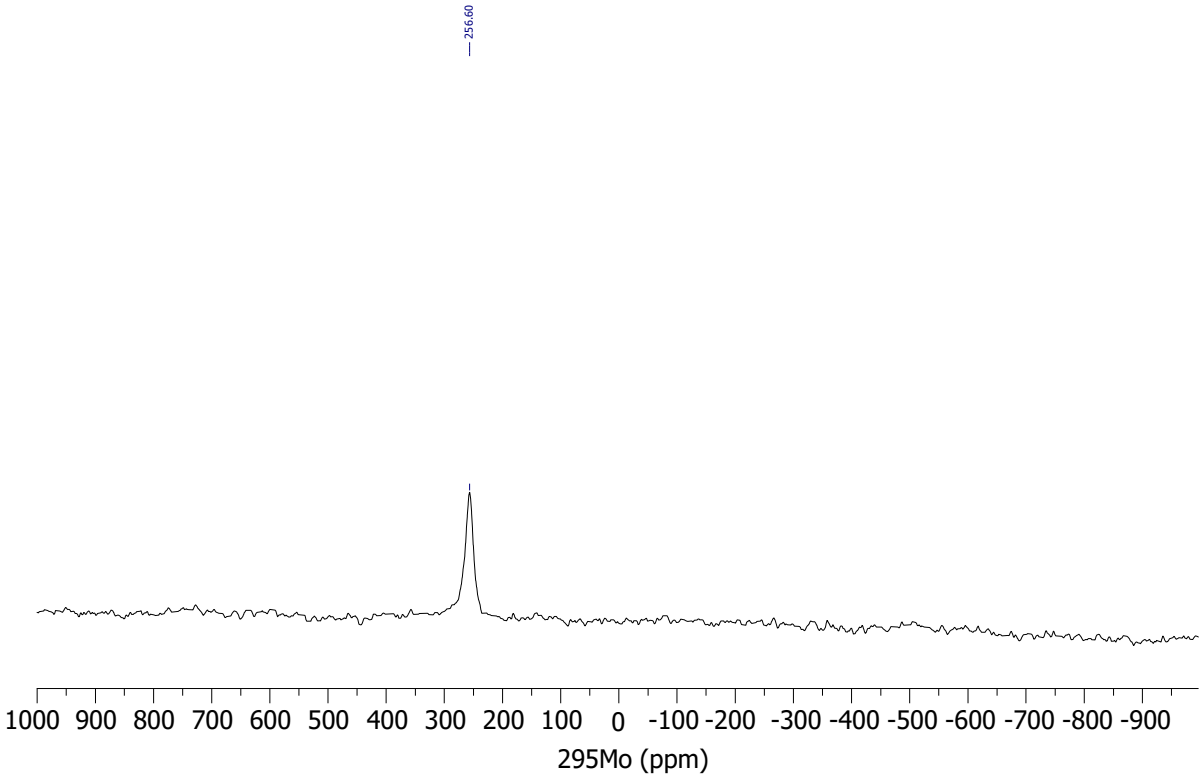

Figure S25: ^{295}Mo NMR (26 MHz) spectrum of [**1**] in CD_2Cl_2.

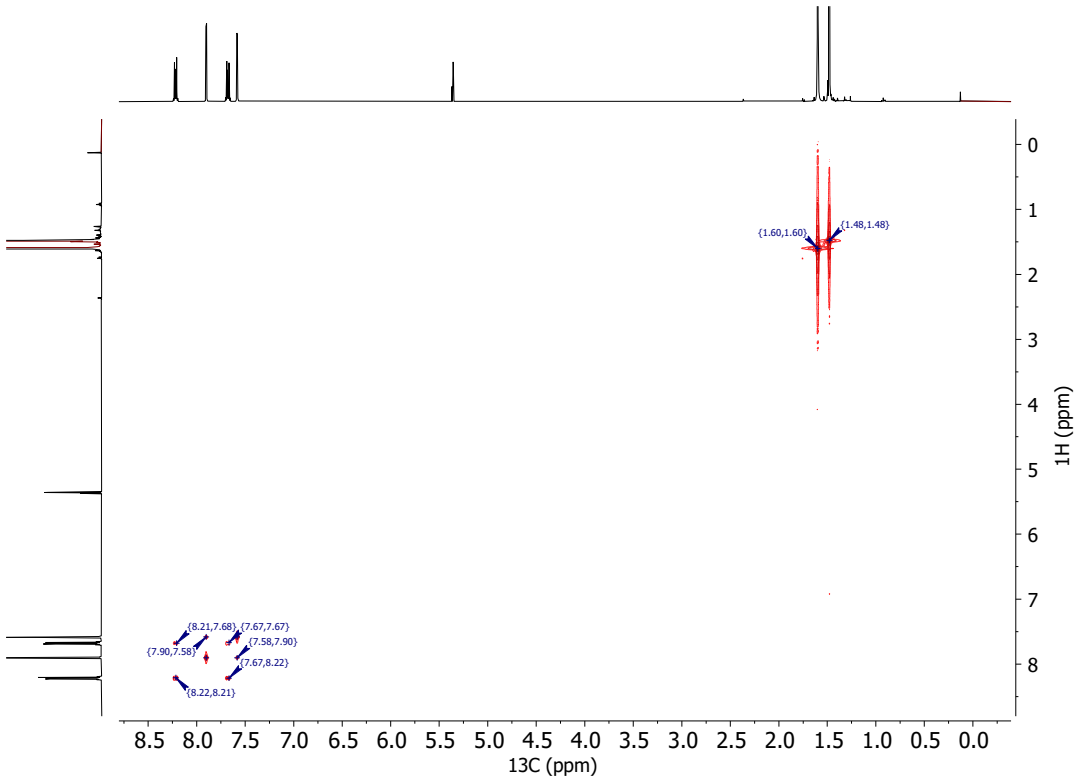

Figure S26: COSY NMR spectrum of [**1**] in CD_2Cl_2.

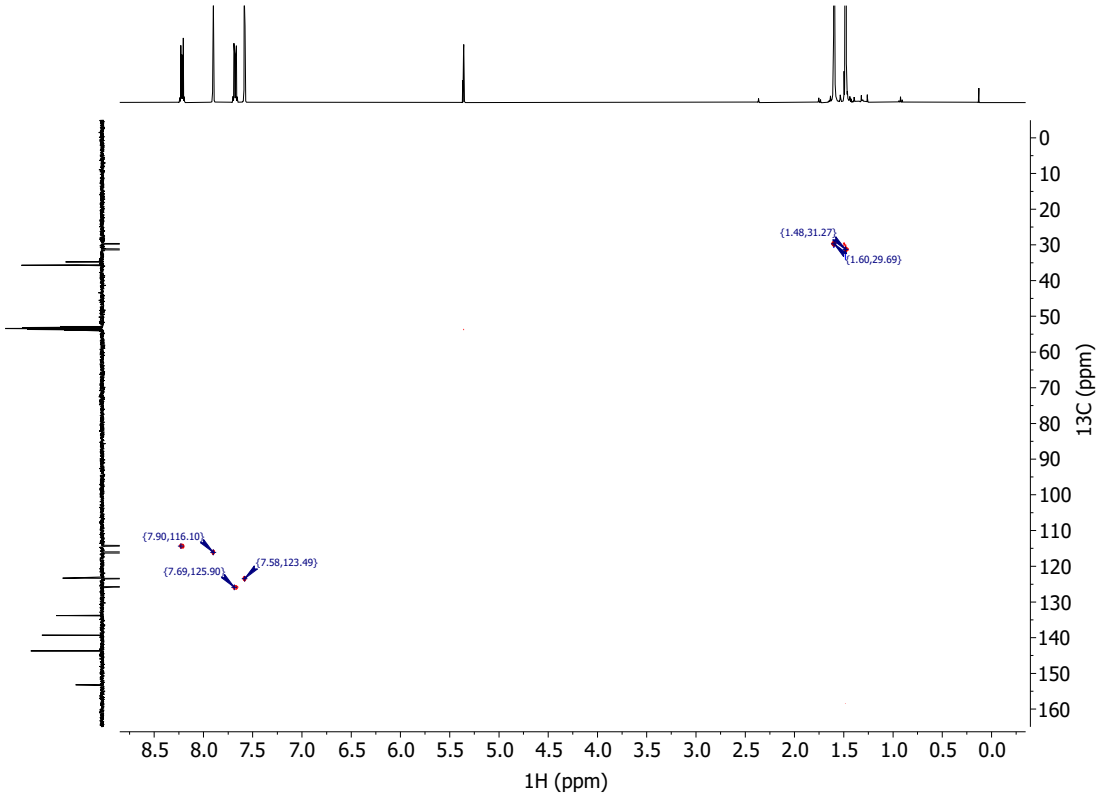

Figure S27: HSQC NMR spectrum of [**1**] in CD_2Cl_2.

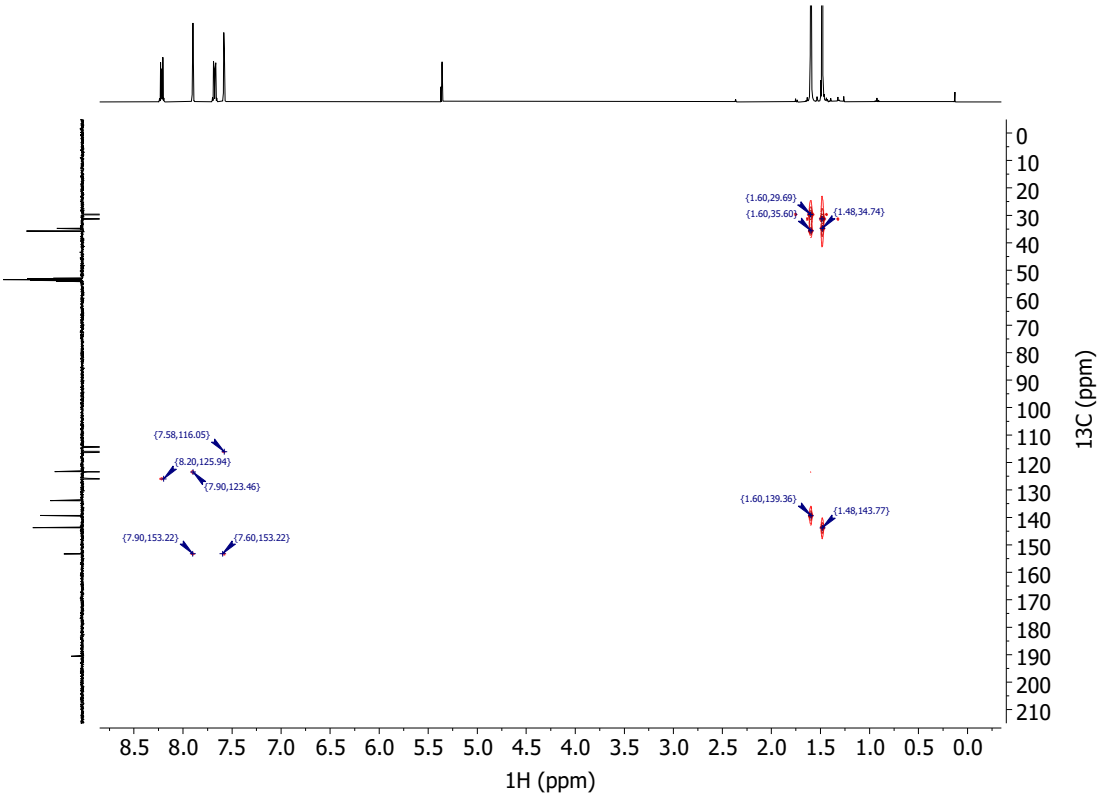

Figure S28: HMBC NMR spectrum of [**1**] in CD_2Cl_2.

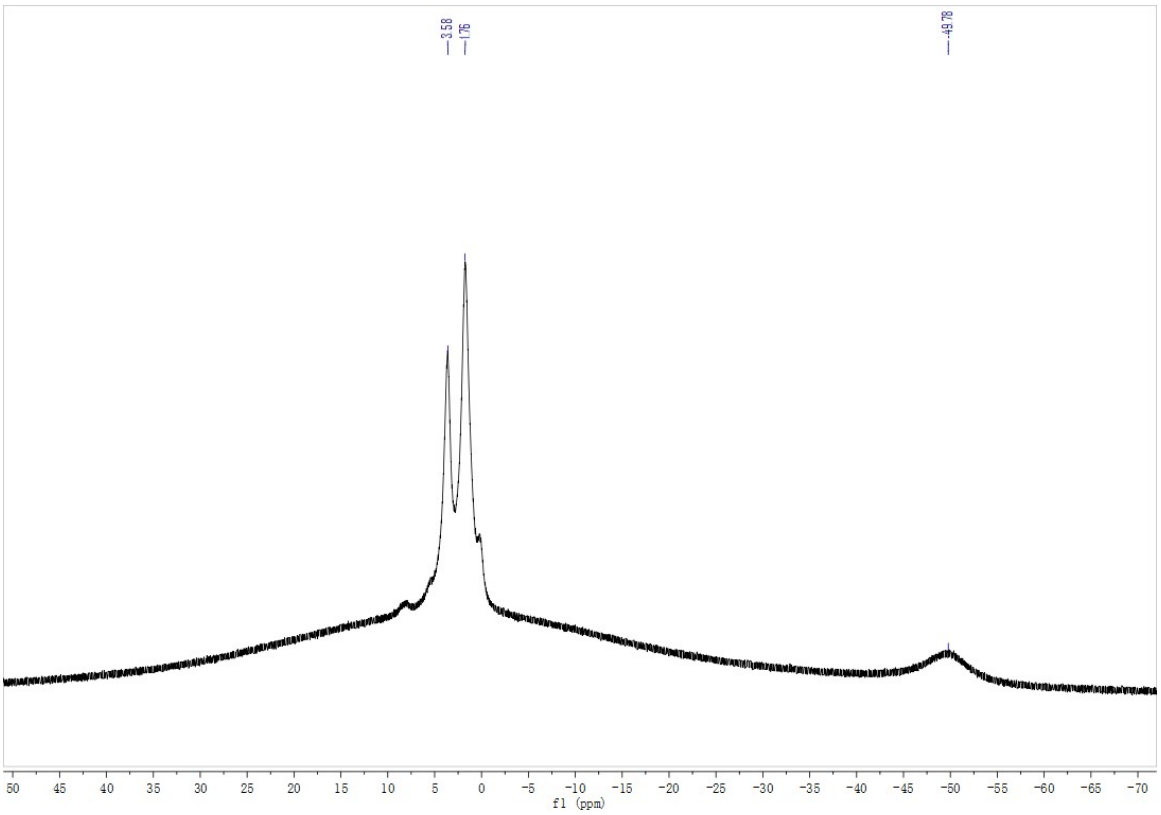

Figure 29: ^{1}H NMR (300 MHz) spectrum of $[1^V]^-Cp_2Co^+$ in THF-d_8.

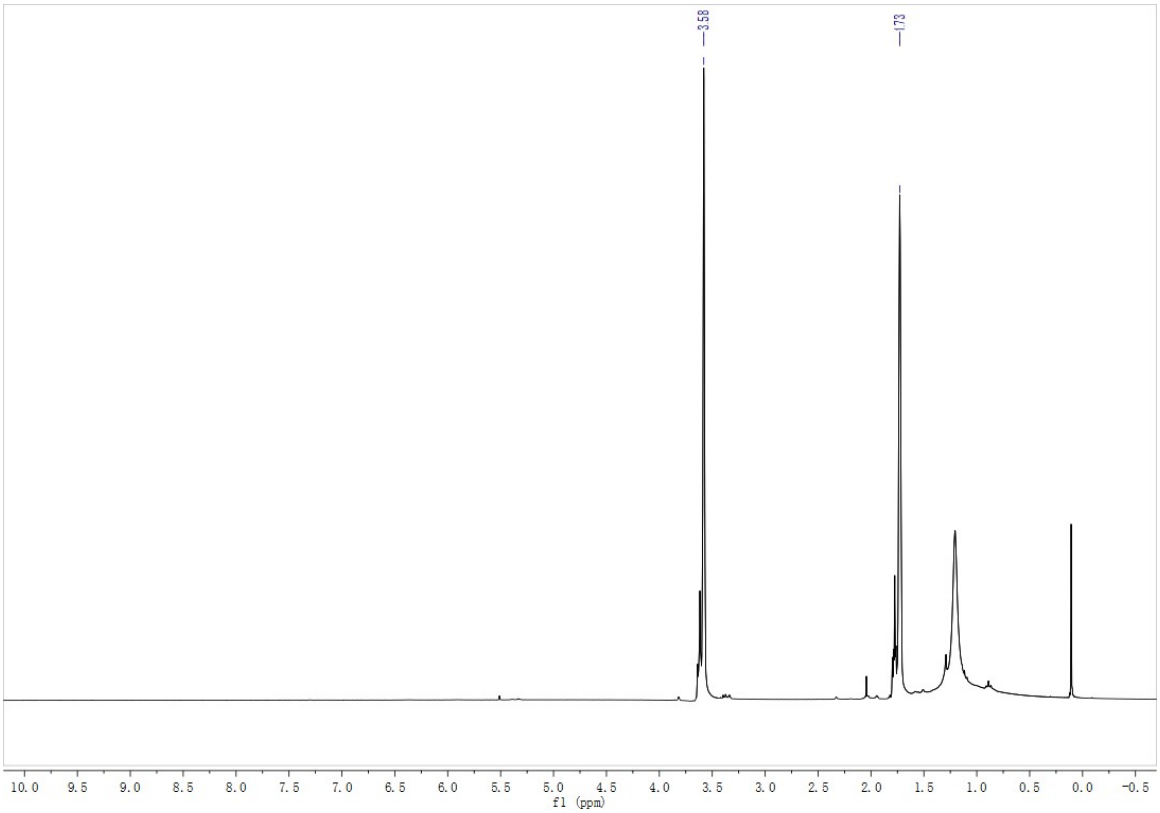

Figure 30: ^{1}H NMR (300 MHz) spectrum of [7] in THF-d_8.

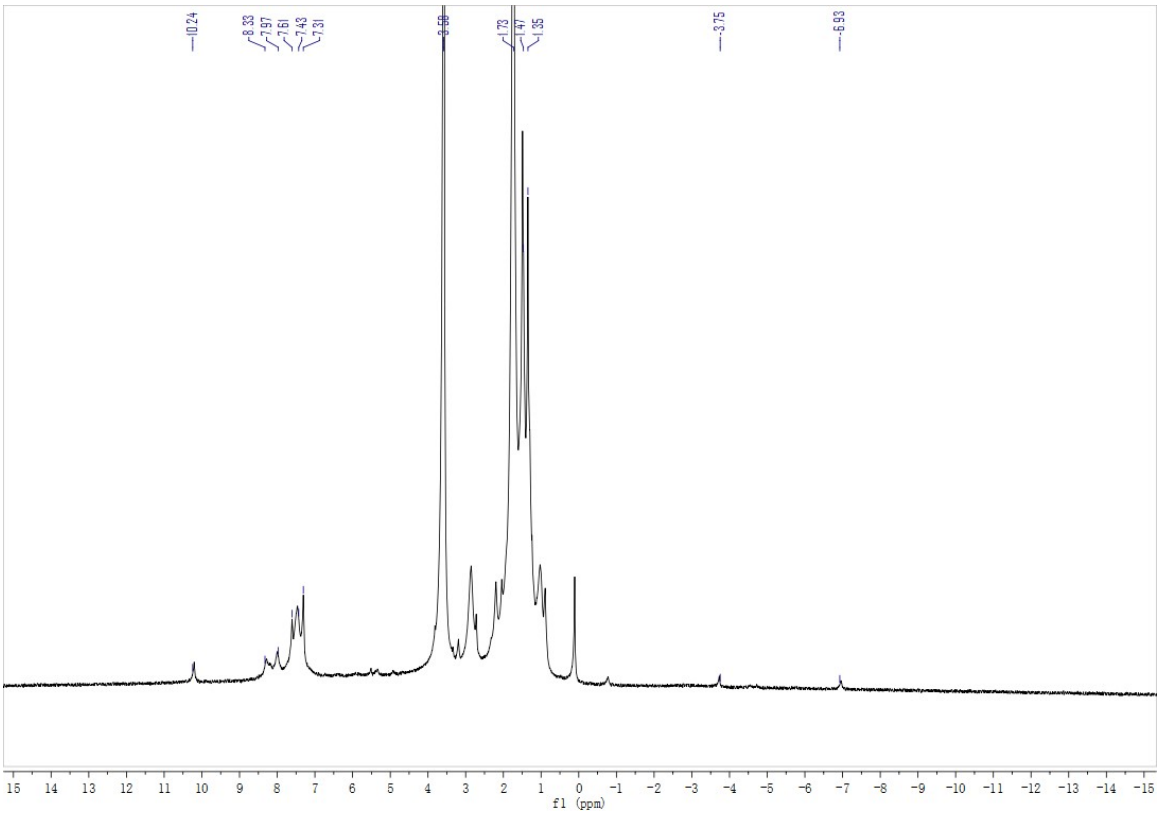

Figure 31: ^{1}H NMR (300 MHz) spectrum of $[7^{IV}]^{-}(C_6H_6)_2Cr^{+}$ in THF-d_8.

Crystallographic data

X-Ray diffraction: The crystal data of complexes **[1^{VI}]**, **[1^{V}]$^{-}$**, **[8$^{V\text{-}IV}$]$^{-}$** , **[7^{IV}]$^{-}$** and **[7^{V}]** were collected on a on a Bruker-AXS D8-Venture diffractometer equipped with a Photon III detector using MoKα radiation (**[1^{VI}]**, **[1^{V}]$^{-}$**, **[7^{IV}]$^{-}$**) or CuKα radiation (**[8$^{V\text{-}IV}$]$^{-}$**) and on a Bruker-AXS D8-Quest diffractometer also equipped with a Photon III detector and a microfocus sealed tube using MoKα radiation (**[7^{V}]**). Phi and omega- scans were used. Crystals were mounted in inert oil and crystal structure determinations were affected at 193K. The data were integrated with SAINT,[6] and an empirical absorption correction with SADABS was applied.[7] The structures were solved using intrinsic phasing method (ShelXT) [8] and refined using the least-squares method on F2 (ShelXL).[9] All non-H atoms were refined with anisotropic displacement parameters. The H atoms were refined isotropically at calculated positions using a riding model, except for H on N atoms (located by difference Fourier maps).

In most structures, some parts (solvent molecules, tButyl groups…) were disordered. Several restraints (SAME, SADI, SIMU, DELU, RIGU, DFIX, ISOR) were applied to refine some moieties of the molecules and to avoid the collapse of the structures during the least-squares refinement by the large anisotropic displacement parameters.

X-ray crystallographic data have been deposited in the Cambridge Crystallographic Data Centre (http://www.ccdc.cam.ac.uk/) with reference numbers: CCDC-2515875 (**[1^{VI}]**), CCDC-2515876 (**[1^{V}]**$^{-}$), CCDC-2515877 (**[8$^{V\text{-}IV}$]**$^{-}$), CCDC-2515878 (**[7^{IV}]**$^{-}$) and CCDC-2515879 (**[7^{V}]**).

These data can be obtained free of charge from https://www.ccdc.cam.ac.uk/structures/ or from the Cambridge Crystallographic Data Centre, 12 Union Road, Cambridge CB2 1EZ, UK; tel: + 44 (0)1223 336408; fax: + 44 (0)1223336033; or e-mail: deposit@ccdc.cam.ac.uk

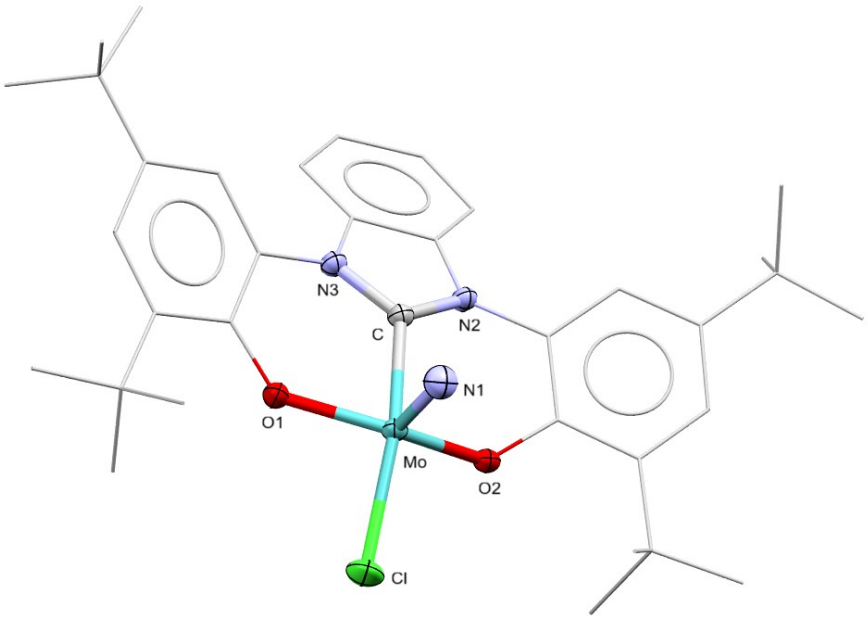

Figure S32: Mercury drawing of [**1^{VI}**]. Hydrogen atoms are omitted for clarity. Ellipsoids are drawn for a 50 % probability.

Table S2: Selected Bond Lengths (Å) and Angles (deg) for [**1^{VI}**]

Mo — N1	1.649(1)
Mo — Cl	2.349(1)
Mo — O1	1.922(1)
Mo — O2	1.921(1)
O1 — Mo — O2	140.7(1)
C — Mo — Cl	157.7(1)

Table S3: X-ray crystallographic data for [**1**^{VI}]

Empirical formula	$C_{35}H_{44}ClMoN_3O_2$	
Formula weight	670.12	
Temperature	193(2) K	
Wavelength	0.71073 Å	
Crystal system	Orthorhombic	
Space group	Pbca	
Unit cell dimensions	*a* = 13.8381(6) Å	α= 90°.
	b = 16.5919(7) Å	β= 90°.
	c = 29.1308(14) Å	γ = 90°.
Volume	6688.4(5) Å^3	
Z	8	
Density (calculated)	1.331 Mg/m^3	
Absorption coefficient	0.506 mm^{-1}	
F(000)	2800	
Crystal size	0.300 x 0.200 x 0.200 mm^3	
Theta range for data collection	2.797 to 30.534°.	
Index ranges	-19≤h≤19, -22≤k≤23, -41≤l≤41	
Reflections collected	310549	
Independent reflections	10200 [R(int) = 0.0345]	
Completeness to theta = 25.242°	99.6 %	
Absorption correction	Semi-empirical from equivalents	
Max. and min. transmission	0.7461 and 0.7073	
Refinement method	Full-matrix least-squares on F^2	
Data / restraints / parameters	10200 / 0 / 391	
Goodness-of-fit on F^2	1.063	
Final R indices [I>2sigma(I)]	R_1 = 0.0269, wR_2 = 0.0670	
R indices (all data)	R_1 = 0.0298, wR_2 = 0.0688	
Extinction coefficient	n/a	
Largest diff. peak and hole	0.511 and -0.62 e.Å^{-3}	

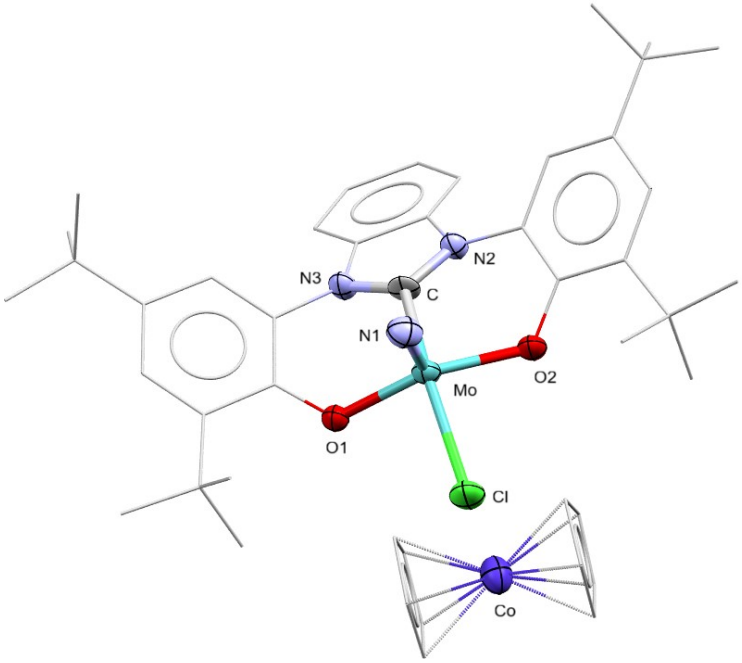

Figure S33: Mercury drawing of [**1**]$^{-}$ Cp_2Co^{+}. Hydrogen atoms are omitted for clarity. Ellipsoids are drawn for a 50 % probability.

Table S4: Selected Bond Lengths (Å) and Angles (deg) for [**1**]$^{-}$ Cp_2Co^{+}

Mo — N1	1.632(6)
Mo — Cl	2.449(2)
Mo — O1	2.052(5)
Mo — O2	2.052(5)
O1 — Mo — O2	139.2(2)
C — Mo — Cl	152.0(2)

Table S5: X-ray crystallographic data for [**1**]$^{-}$ Cp_2Co^{+}

Empirical formula	$C_{49}H_{60}ClCoMoN_5O_2$	
Formula weight	941.34	
Temperature	193(2) K	
Wavelength	0.71073 Å	
Crystal system	Monoclinic	
Space group	Cc	
Unit cell dimensions	a = 9.6168(6)Å	α= 90°.
	b = 22.4885(14)Å	β= 90.055(2)°.
	c = 21.3839(12)Å	γ = 90°.
Volume	4624.6(5)Å^3	
Z	4	
Density (calculated)	1.352 Mg/m^3	
Absorption coefficient	0.731 mm^{-1}	
F(000)	1964	
Crystal size	0.12×0.14×0.15 mm^3	
2 Theta range for data collection	5.72 to 55.06 (0.77 Å)°.	
Index ranges	-12≤h≤12, -29≤k≤29, -27≤l≤26	
Reflections collected	77274	
Independent reflections	10097 [R(int) = 0.1066]	
Completeness to theta = 25.242°	99.8 %	
Absorption correction	Semi-empirical from equivalents	
Max. and min. transmission	0.7314 and 0.6730	
Refinement method	Full-matrix least-squares on F^2	
Data / restraints / parameters	10097 / 943 / 745	
Goodness-of-fit on F^2	1. 026	
Final R indices [I>2sigma(I)]	R_1 = 0.0391 wR_2 = 0.0703	
R indices (all data)	R_1 = 0. 0570, wR_2 = 0. 0767	
Absolute structure parameter	-0.254(16)	
Extinction coefficient	n/a	
Flack X parameter	0.02(1)	
Largest diff. peak and hole	0.40/−0.31 e.Å^{-3}	

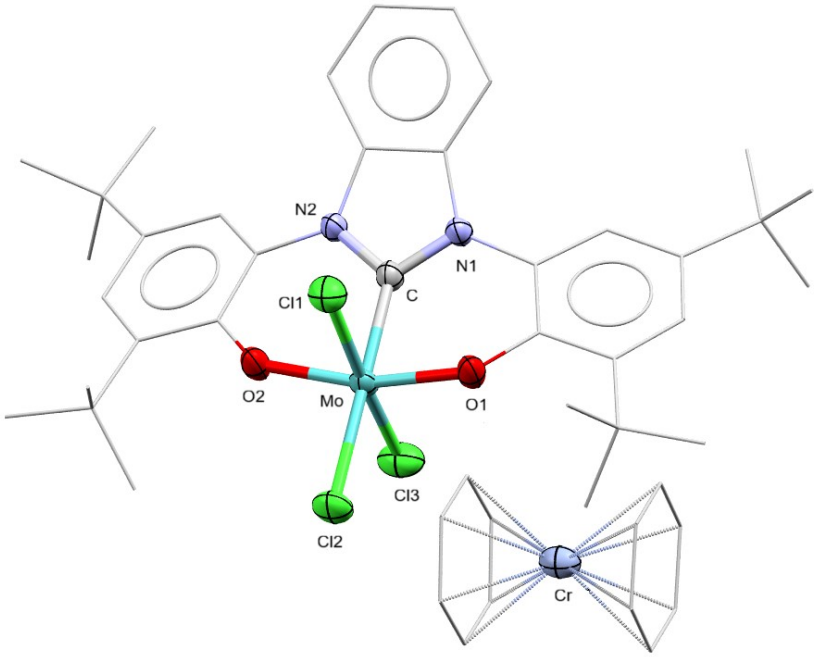

Figure S34: Mercury drawing of [**7**]$^-$. Hydrogen atoms are omitted for clarity. Ellipsoids are drawn for a 50 % probability.

Table S6: Selected Bond Lengths (Å) and Angles (deg) for [**7**]$^-$

Mo — Cl1	2.471(1)
Mo — Cl2	2.400(1)
Mo — Cl3	2.464(1)
Mo — O1	1.905(2)
Mo — C	2.109(3)
O1 — Mo — O2	164.6(1)
C — Mo — Cl2	179.6(1)

Table S7: X-ray crystallographic data for [**7**]$^-$

Empirical formula	$C_{50}H_{59}Cl_{12}CrMoN_2O_2$	
Formula weight	1293.33	
Temperature	193(2) K	
Wavelength	0.71073 Å	
Crystal system	Orthorhombic	
Space group	Pnma	
Unit cell dimensions	a = 16.3990(7) Å	α= 90°.
	b = 20.0066(10) Å	β= 90°.
	c = 17.6816(9) Å	γ = 90°.
Volume	5801.1(5) Å^3	
Z	4	
Density (calculated)	1.481 Mg/m^3	
Absorption coefficient	0.995 mm^{-1}	
F(000)	2636	
Crystal size	0.260 x 0.160 x 0.120 mm^3	
Theta range for data collection	2.617 to 28.353°.	
Index ranges	-21≤h≤21, -26≤k≤26, -23≤l≤23	
Reflections collected	193248	
Independent reflections	7422 [R(int) = 0.1190]	
Completeness to theta = 25.242°	99.9 %	
Absorption correction	Semi-empirical from equivalents	
Max. and min. transmission	0.7457 and 0.5552	
Refinement method	Full-matrix least-squares on F^2	
Data / restraints / parameters	7422 / 366 / 408	
Goodness-of-fit on F^2	1.057	
Final R indices [I>2sigma(I)]	R_1 = 0.0425, wR_2 = 0.1037	
R indices (all data)	R_1 = 0.0650, wR_2 = 0.1200	
Extinction coefficient	n/a	
Largest diff. peak and hole	0.698 and -0.753 e.Å^{-3}	

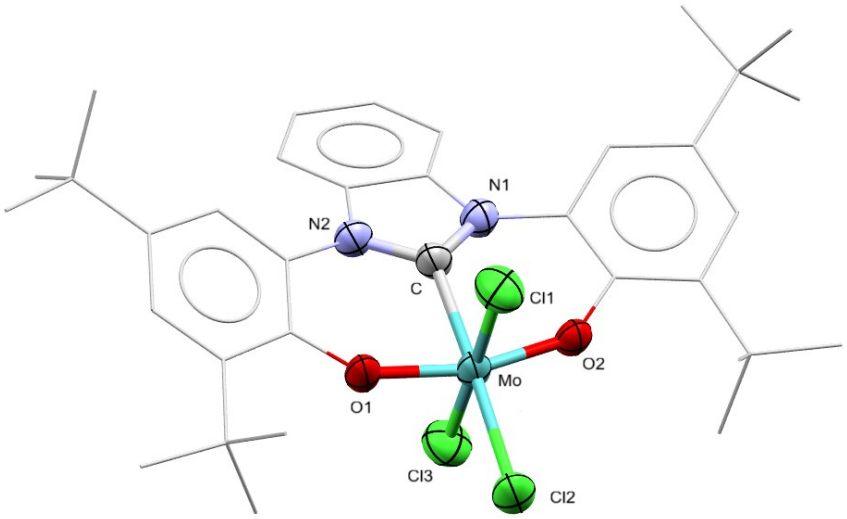

Figure S35: Mercury drawing of [**7**]. Hydrogen atoms are omitted for clarity. Ellipsoids are drawn for a 50 % probability.

Table S8: Selected Bond Lengths (Å) and Angles (deg) for [**7**]

Mo — Cl1	2.360(1)
Mo — Cl2	2.360(1)
Mo — Cl3	2.395(1)
Mo — O1	1.837(3)
Mo — C	2.167(4)
O1 — Mo — O2	161.6(1)
C — Mo — Cl2	175.9(1)

Table S9: X-ray crystallographic data for [**7**]

Empirical formula	$C_{39}H_{52}Cl_3MoN_2O_3$	
Formula weight	799.11	
Temperature	193(2) K	
Crystal system	monoclinic	
Space group	$P2_1/n$ (14)	
Unit cell dimensions	a = 10.1180(5) Å	α= 90°.
	b = 18.3140(8) Å	β= 90°.
	c = 21.4097(9) Å	γ = 90°.
Volume	3967.2(3) $Å^3$	
Z	4	
Density (calculated)	1.338 Mg/m^3	
Absorption coefficient	4.852 mm^{-1}	
F(000)	1668	
Crystal size	0.06×0.18×0.25 mm^3	
Theta range for data collection	4.13 to 134.06°.	
Index ranges	-12≤ h≤12, -21≤k≤20, -25≤l≤25	
Reflections collected	86557	
Independent reflections	7030 [R(int) = 0.0803]	
Completeness to theta = 25.242°	99.4 %	
Data / restraints / parameters	7030 / 358 / 517	
Goodness-of-fit on F^2	1.057	
Final R indices [I>2sigma(I)]	R_1 = 0.0481, wR_2 = 0.1276	
R indices (all data)	R_1 = 0.0519, wR_2 = 0.1326	
Largest diff. peak and hole	0.86 and -0.81 e.$Å^{-3}$	

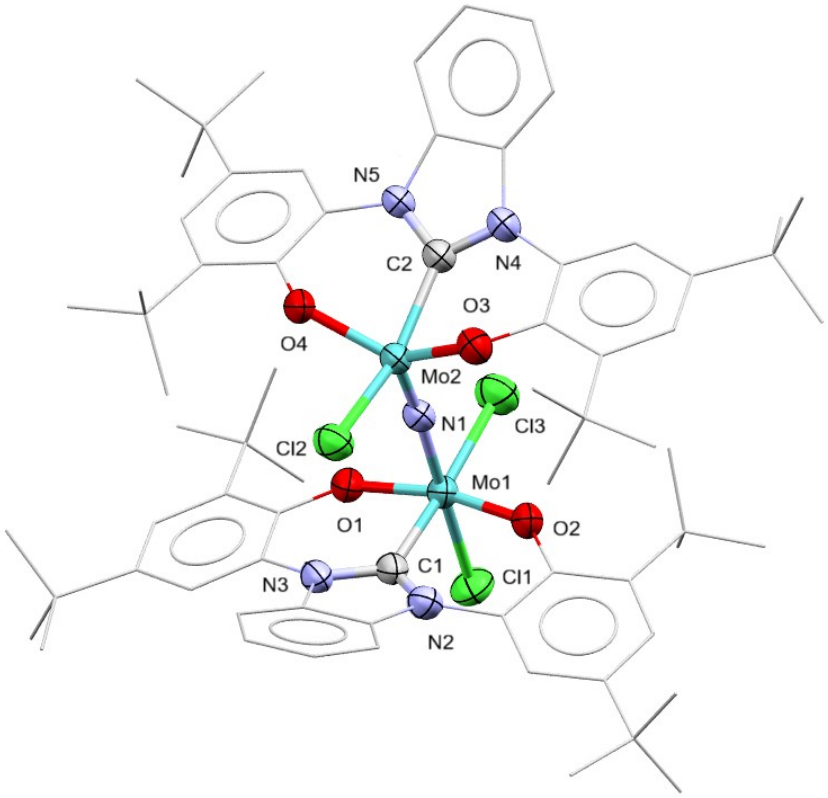

Figure S36: Mercury drawing of [**8**]$^{-}$. Hydrogen atoms are omitted for clarity. Ellipsoids are drawn for a 50 % probability.

Table S10: Selected Bond Lengths (Å) and Angles (deg) for [**8**]$^{-}$

Mo1 — N1	2.020(2)
Mo2 — N1	1.702(2)
Mo2 — Cl2	2.434(1)
Mo1 — Cl1	2.497(1)
Mo1 — Cl3	2.444(1)
Mo2 — C2	2.137(3)
Mo1 — N1 — Mo1	174.2(2)
N1 — Mo1 — Cl1	179.7(1)
N1 — Mo2 — Cl2	102.5(1)

Table S11: X-ray crystallographic data for [**8**]$^-$

Empirical formula	$C_{215}H_{308}Cl_6Co_2Mo_4N_{10}O_{20}$
Formula weight	4067.02
Temperature [K]	193(2)
Crystal system	monoclinic
Space group (number)	$P2_1/n$ (14)
a [Å]	14.7494(5)
b [Å]	24.7702(9)
c [Å]	30.2705(11)
α [°]	90
β [°]	93.023(2)
γ [°]	90
Volume [Å^3]	11043.8(7)
Z	2
ρ_{calc} [gcm^{-3}]	1.223
μ [mm^{-1}]	4.092
F(000)	4304
Crystal size [mm^3]	0.12×0.25×0.25
Crystal colour	red
Crystal shape	plate
Radiation	CuK_α (λ=1.54178 Å)
2θ range [°]	6.81 to 140.75 (0.82 Å)
Index ranges	−16 ≤ h ≤ 17
	−29 ≤ k ≤ 30
	−36 ≤ l ≤ 36
Reflections collected	287171
Independent reflections	21010
	R_{int} = 0.0871
	R_{sigma} = 0.0519
Completeness to θ = 67.679°	99.9
Data / Restraints / Parameters	21010 / 2940 / 1727
Goodness-of-fit on F^2	1.027
Final *R* indexes [$I \geq 2\sigma(I)$]	R_1 = 0.0473, wR_2 = 0.1316
R indices (all data)	R_1 = 0.0559, wR_2 = 0.1392
Largest diff. peak and hole	0.59 and −0.74e.Å^{-3}

Computational Details

Geometry optimizations were performed using Gaussian 16 (Revision C01)[10] at the PBE0 level of hybrid density functional theory,[11] with inclusion of D3(bj) corrections in the optimization process.[12,13] The geometries of all located extrema are given as xyz coordinates data in a separate file (Geom.xyz) in the SI. The atoms Cl, C, H, N, O and P were represented by an svp basis set.[14] The Mo atom was represented by Dolg's pseudo potential and the associated basis set.[15,16] The solvent (acetonitrile) influence was taken into consideration both during the optimization process and through single-point calculations on the optimized geometries with the SMD model.[17] For the SP calculations, the atoms were treated with a def2-qzvp basis set.[18] All energies reported are Gibbs free energies obtained at 298 K and 1atm using a procedure described by Ariai and Gellrich in a recent paper to better described the entropy penalty for associative reactions.[19] The procedure described by equation 14 in Ref 19 has been considered : E_{elst} is obtained in single point calculations with implicit inclusion of the solvent (ACN) by substracting the non-electrostatic component from the converged energy. The entropy contribution of each species is computed from the frequency calculations output using a script obtained from the authors of reference 19.

Table S12: Energies of all computed compounds of the present study

	E(smd/def2-qzvp) (au)	**nes term (kcal/mol)**	**E(smd) + nes (au)**	**S(sol) cal/(K*mol)**	**G (kcal/mol)**
Fc^+	-1650.178916	-2.67	-1650.174661	44.447	-1035513.677
Fc	-1650.36211	-2.67	-1650.357855	44.445	-1035628.633
$CoCp_2^+$	-1769.275572	-2.67	-1769.271317	44.508	-1110247.989
$CoCp_2$	-1769.402552	-2.7	-1769.398249	44.499	-1110327.637
$CoCp^*_2{}^+$	-2162.191492	-2.55	-2162.187428	46.208	-1356807.124
$CoCp^*_2$	-2162.289669	-2.59	-2162.285542	46.186	-1356868.684
LutH	-327.1571053	-1.5	-327.1547149	41.946	-205305.2272
Lut	-326.6907907	-1.25	-326.6887987	41.824	-205012.824
H	-0.500892656	0.46	-0.501625713	9.112	-317.491688
Cl^-	-460.2453911	-1.06	-460.2437019	18.516	-288812.8572
CH_3CN	-132.662284	1.21	-132.6642123	32.495	-83257.75383
NH_3	-56.52613633	1.72	-56.52887732	26.494	-35480.31182
NH_4^+	-56.99196283	1.36	-56.99413013	24.706	-35771.72932
N_2	-109.4464571	3.57	-109.4521462	26.661	-68690.22039

[1^{VI}] (S=0)	-2202.28263	-5.79	-2202.273403	44.789	-1381961.034
[1^{VI}] (S=T)	-2202.239867	-5.82	-2202.230592	44.642	-1381934.126
[1^{V}]$^{-}$ (S=1/2)	-2202.423477	-5.75	-2202.414314	44.69	-1382049.428
[1^{V}]$^{-}$ (S=3/2)	-2202.323951	-5.77	-2202.314756	44.603	-1381986.928
[2^{V}] (S=1/2)	-2202.88698	-6.13	-2202.877211	44.777	-1382339.926
[2^{V}] (S=3/2)	-2202.813567	-6.05	-2202.803926	44.723	-1382293.922
[3^{IV}] (S=0)	-2203.487492	-6.22	-2203.47758	44.87	-1382716.691
[3^{IV}] (S=1)	-2203.497831	-6.25	-2203.487871	44.82	-1382723.133
[4^{IV}] (S=0)	-2664.240958	-6.77	-2664.23017	45.201	-1671843.458
[4^{IV}] (S=1)	-2664.241845	-6.84	-2664.230944	45.096	-1671843.913
[5^{IV}]$^{+}$ (S=0)	-2203.954289	-6.49	-2203.943947	45.046	-1383009.393
[5^{IV}]$^{+}$ (S=1)	-2203.952382	-6.43	-2203.942135	45.057	-1383008.259
[6^{IV}]$^{-}$ (S=0)	-2663.750487	-6.61	-2663.739954	45.099	-1671535.813
[6^{IV}]$^{-}$ (S=1)	-2663.758401	-6.58	-2663.747915	45.004	-1671540.78
[7^{IV}]$^{-}$ (S=0)	-3067.949008	-7.86	-3067.936482	45.01	-1925172.984
[7^{IV}]$^{-}$ (S=1)	-3067.955771	-7.91	-3067.943166	45.016	-1925177.18
[A] (S=0)	-2607.665292	-7.64	-2607.653117	44.826	-1636340.703
[A] (S=1)	-2607.667005	-7.79	-2607.65459	44.762	-1636341.609
[B] (S=0)	-2717.130655	-5.3	-2717.122209	45.116	-1705033.695
[B] (S=1)	-2717.124517	-5.4	-2717.115912	45.012	-1705029.712
[9^{III}]$^{-}$ (S=1/2)	-2717.269991	-5.4	-2717.261385	45.016	-1705120.999
[9^{III}]$^{-}$ (S=3/2)	-2717.264781	-5.41	-2717.256159	44.986	-1705117.711
[10^{III}] (S=1/2)	-2256.997315	-5	-2256.989347	44.928	-1416295.855
[10^{III}] (S=3/2)	-2256.981792	-5.09	-2256.97368	44.829	-1416285.995
[$12^{III\text{-}III}$]	-4404.582531	-11.27	-4404.564571	43.506	-2763919.479
TS N_2 spliting					
(i=-793 cm-1)	-4404.53316	-10.99	-4404.515646	43.546	-2763888.79

Note: i=-793 cm-1 is the imaginary frequency of the computed TS for N_2 splitting.

References

(1) DiFranco. S. A.; Maciulis. N. A.; Staples. R. J.; Batrice. R. J.; Odom. A. L. Evaluation of Donor and Steric Properties of Anionic Ligands on High Valent Transition Metals. *Inorg. Chem.* **2012**. *51* (2). 1187–1200.

(2) Curley. J. J.; Bergman. R. G.; Tilley. T. D. Preparation and Physical Properties of Early-Late Heterobimetallic Compounds Featuring Ir–M Bonds (M = Ti. Zr. Hf). *Dalton Trans.* **2011**. *41* (1). 192–200.

(3) Garrido-Barros. P.; Derosa. J.; Chalkley. M. J.; Peters. J. C. Tandem Electrocatalytic N_2 Fixation via Proton-Coupled Electron Transfer. *Nature* **2022**. *609* (7925). 71–76.

(4) Stoll. S.; Schweiger. A. EasySpin. A Comprehensive Software Package for Spectral Simulation and Analysis in EPR. *J. Magn. Reson.* **2006**. *178* (1). 42–55.

(5) Feltham. R. D. Electron Spin Resonance and Optical Spectra of Chromium “Sandwich” Compounds. *J. Inorg. Nucl. Chem.* **1961**. *16* (3–4). 197–203.

[6] SAINT. Program for Data Reduction. Bruker-AXS. **2008**.

[7] Bruker. SADABS. Bruker AXS Inc. Program for Data Correction. **2006**.

[8] G. M. Sheldrick. *Acta Crystallogr. Sect. A Found. Crystallogr*. **2015**. *71*. 3–8.

[9] G. M. Sheldrick. *Acta Crystallogr. Sect. C Struct. Chem.* **2015**. *71*. 3–8.

[10] M. J. Frisch. G. W. Trucks. H. B. Schlegel. G. E. Scuseria. M. A. Robb. J. R. Cheeseman. G. Scalmani. V. Barone. G. A. Petersson. H. Nakatsuji. X. Li. M. Caricato. A. V. Marenich. J. Bloino. B. G. Janesko. R. Gomperts. B. Mennucci. H. P. Hratchian. J. V. Ortiz. A. F. Izmaylov. J. L. Sonnenberg. D. Williams-Young. F. Ding. F. Lipparini. F. Egidi. J. Goings. B. Peng. A. Petrone. T. Henderson. D. Ranasinghe. V. G. Zakrzewski. J. Gao. N. Rega. G. Zheng. W. Liang. M. Hada. M. Ehara. K. Toyota. R. Fukuda. J. Hasegawa. M. Ishida. T. Nakajima. Y. Honda. O. Kitao. H. Nakai. T. Vreven. K. Throssell. J. Montgomery. J. A.. J. E. Peralta. F. Ogliaro. M. J. Bearpark. J. J. Heyd. E. N. Brothers. K. N. Kudin. V. N. Staroverov. T. A. Keith. R. Kobayashi. J. Normand. K. Raghavachari. A. P. Rendell. J. C. Burant. S. S. Iyengar. J. Tomasi. M. Cossi. J. M. Millam. M. Klene. C. Adamo. R. Cammi. J. W. Ochterski. R. L. Martin. K. Morokuma. O. Farkas. J. B. Foresman. D. J. Fox. **2016**.

[11] C. Adamo. V. Barone. Toward Reliable Density Functional Methods Without Adjustable Parameters: The PBE0 Model. *J. Chem. Phys.* **1999**. *110*. 6158–6170.

[12] S. Grimme. J. Antony. S. Ehrlich. H. Krieg. A Consistent and Accurate ab Initio Parametrization of Density Functional Dispersion Correction (DFT-D) for the 94 Elements H-Pu. *J. Chem. Phys.* **2010**. *132*. *154104*.

[13] S. Grimme. S. Ehrlich. L. Goerigk. Effect of the Damping Function in Dispersion Corrected Density Functional Theory. *J. Comput. Chem.* **2011**. *32*. 1456–1465.

[14] A. Schäfer. H. Horn. R. Ahlrichs. Fully Optimized Contracted Gaussian Basis Sets for Atoms Li to Kr. *J. Chem. Phys.* **1992**. *97*. 2571–2577.

[15] D. Andrae. U. Häußermann. M. Dolg. H. Stoll. H. Preuß. Theor. Energy-adjusted ab Initio Pseudopotentials for the Second and Third Row Transition Elements. *Chim. Acta.* **1990**. *77*. 123–141.

[16] K. A. Peterson. D. Figgen. E. Goll. H. Stoll. M. Dolg. Systematically Convergent Basis Sets with Relativistic Pseudopotentials. II. Small-core Pseudopotentials and Correlation Consistent Basis Sets for the Post-d Group 16–18 Elements. *J. Chem. Phys.* **2003**. *119*. 11113–11123.

[17] A. V. Marenich. C. J. Cramer. D. G. Truhlar. Universal Solvation Model Based on Solute Electron Density and on a Continuum Model of the Solvent Defined by the Bulk Dielectric Constant and Atomic Surface Tensions. *J. Phys. Chem. B* **2009**. *113*. 6378–6396.

[18] F. Weigend. R. Ahlrichs. Balanced Basis Sets of Split Valence, Triple Zeta Valence and Quadruple Zeta Valence Quality for H to Rn: Design and Assessment of Accuracy. *Phys. Chem. Chem. Phys.* **2005**. *7*. 3297–3305.

[19] J. Ariai. U. Gellrich. The Entropic Penalty for Associative Reactions and Their Physical Treatment during Routine Computations. *Phys. Chem. Chem. Phys.* **2023**. *25*. 14005-14015.